
Mantis: Lightweight Calibrated Foundation Model for User-Friendly Time Series Classification

Vasilii Feofanov, Songkang Wen, Marius Alonso, Romain Ilbert, Hongbo Guo,
Malik Tiomoko, Lujia Pan, Jianfeng Zhang, Ievgen Redko

Huawei Noah's Ark Lab

Correspondance to vasilii.feofanov@huawei.com

Abstract

In recent years, there has been increasing interest in developing foundation models for time series data that can generalize across diverse downstream tasks. While numerous forecasting-oriented foundation models have been introduced, there is a notable scarcity of models tailored for time series classification. To address this gap, we present **Mantis**, a new open-source foundation model for time series classification based on the Vision Transformer (ViT) architecture that has been pre-trained using a contrastive learning approach. Our experimental results show that Mantis outperforms existing foundation models both when the backbone is frozen and when fine-tuned, while achieving the lowest calibration error. In addition, we propose several adapters to handle the multivariate setting, reducing memory requirements and modeling channel interdependence.

Mantis  <https://github.com/vfeofanov/mantis>

1 Introduction

The advent of large foundation models (Bommasani et al., 2021) in computer vision (He et al., 2015; Dosovitskiy et al., 2021) and natural language processing (Achiam et al., 2023; Touvron et al., 2023) has significantly transformed research and applications. These models are pre-trained on extensive, diverse datasets to generalize across a wide range of downstream tasks. This approach not only simplifies model architecture selection but also reduces the need for large amounts of labeled data for new tasks, as the foundation model leverages its previously acquired knowledge.

Over the past two years, the development of time series foundation models (TSFMs) has emerged as a prominent research area. For time series forecasting, numerous models have been proposed, either pre-trained from scratch on large volumes of time series data (Rasul et al., 2023; Das et al., 2023; Woo et al., 2024; Wang et al., 2024), including synthetic time series (Ansari et al., 2024; Bhethanabhotla et al., 2024), or adapted from pre-trained large language models (LLMs, Jin et al., 2023; Chang et al., 2023; Cao et al., 2023; Xue and Salim, 2023; Gruver et al., 2024).

Some foundation models are designed to handle multiple tasks simultaneously, such as forecasting, classification, imputation, and anomaly detection (Zhou et al., 2023; Goswami et al., 2024). However, these general-purpose models may exhibit suboptimal performance because certain pre-training schemes are inherently more suitable for specific tasks (e.g., masked reconstruction loss may be better suited for imputation, while contrastive loss aligns more naturally with classification). Surprisingly, despite the widespread use of time series classification (Bagnall et al., 2018; Dau et al., 2019; Dempster et al., 2020), relatively few models focus specifically on this task. To address this gap, we developed Mantis, a new time series classification foundation model:

Our goal is to provide an open-source, lightweight, and high-performance model that can be readily used by practitioners and researchers across diverse domains.

The design of Mantis draws from advancements in time series representation learning (Yue et al., 2022; Eldele et al., 2021; Zhang et al., 2022), transformer-based models for time series (Nie et al., 2023; Ilbert et al., 2024; Lin et al., 2024). The architecture of our model (Figure 1) features a token generator that transforms time series data into meaningful

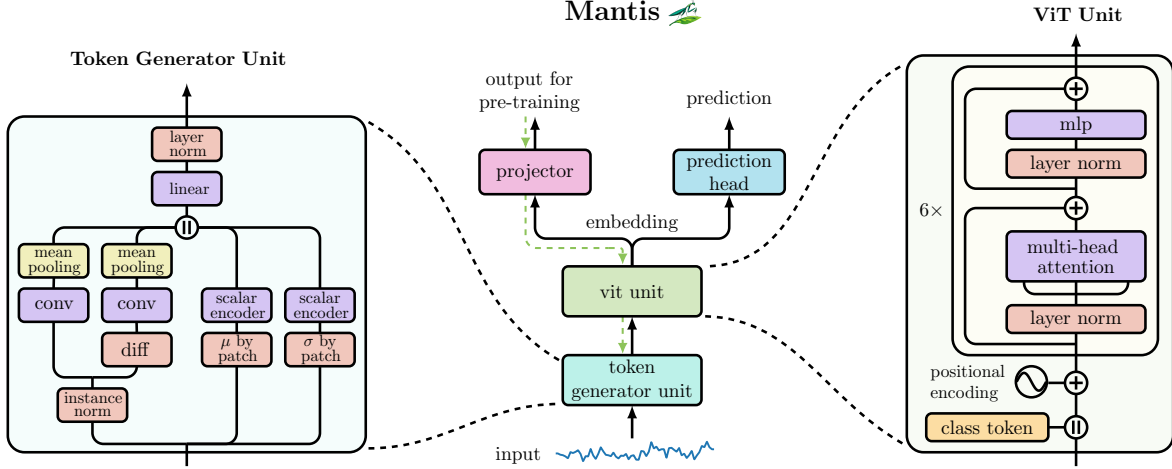


Figure 1: Architecture. By symbol $+$ we denote the sum operator, while $||$ designates the vector concatenation operator.

patches and a Vision Transformer (ViT) component similar to [Dosovitskiy et al. \(2021\)](#). We contrastively pre-trained Mantis on 7 million time series samples, resulting in a model with 8 million parameters. The pre-trained checkpoint is open-sourced on [HuggingFace](#), and our [GitHub package](#) includes an API for inference and fine-tuning on new downstream tasks. We perform extensive experiments to demonstrate the superiority of Mantis, while also showing that our model is the most calibrated compared to other time series classification foundation models.

Another challenge addressed in this work is that Mantis, like most existing TSFMs, is designed for univariate time series, whereas many real-world applications involve observations with multiple time series channels ([Wei, 2018](#)). A straightforward approach in such cases is to apply a TSFM independently to each channel. However, this method has significant drawbacks when working with datasets containing hundreds or thousands of channels ([Bagnall et al., 2018](#)). Treating channels independently results in increased runtime and memory consumption, making TSFMs less practical for environments with limited computational resources. To address this limitation, we provide Mantis with several adapters that compress the original channels into a smaller number of new channels, which are then processed by the foundation model. Our experiments demonstrate that these adapters not only substantially improve inference speed but also enable efficient fine-tuning of Mantis for tasks involving a very large number of channels.

2 Methodology

In this section, we present the main technical details behind Mantis: we mathematically introduce the problem setup, discuss the data pre-processing, and present the architecture and the pre-training process.

2.1 Problem Setup

Mathematically speaking, our time series classification foundation model is an encoder $F : \mathbb{R}^t \rightarrow \mathbb{R}^q$ that projects any time series $\mathbf{x} \in \mathbb{R}^t$ with a fixed sequence length t to a discriminative hidden space \mathbb{R}^q . During the pre-training phase, we observe an unlabeled pre-training set X_0 that is sufficiently large in order to learn rich embeddings that generalize well across different tasks. During the fine-tuning phase, we observe a supervised downstream task with observations X and labels Y . The two options are possible: 1) we use F to extract deep embeddings $Z = \{F(\mathbf{x}), \mathbf{x} \in X\}$ and then learn any classifier $h : \mathbb{R}^q \rightarrow \{1, \dots, K\}$ using Z as features and Y as corresponding labels, 2) append a classification head $h : \mathbb{R}^q \rightarrow \mathbb{R}^K$ and fine-tune $h \circ F$ by minimizing a loss function evaluated on the downstream dataset.

When time series with multiple channels $\mathbf{x} = [\mathbf{x}_1, \dots, \mathbf{x}_d] \in \mathbb{R}^{d \times t}$, $d > 1$, are considered, we send each channel \mathbf{x}_i , $i \in [1, d]$, to the TSFM independently, i.e., the embedding of \mathbf{x} is defined as $\mathbf{z} = \text{concat}[(F(\mathbf{x}_i))_{1 \leq i \leq d}]$, where concat denotes the vector concatenation operator, and the input dimension of the classifier (head) is $\mathbb{R}^{d \times q}$. As we will discuss in Section 2.5, when d is large, we can employ an adapter $a : \mathbb{R}^{d \times t} \rightarrow \mathbb{R}^{d_{\text{new}} \times t}$ that compresses the original channels into new d_{new} channels. In this case, the embedding \mathbf{z} is calculated as $\mathbf{z} = \text{concat}[(F(a(\mathbf{x})_i))_{1 \leq i \leq d_{\text{new}}}]$, where $a(\mathbf{x})_i$ denotes the i -th new channel.

Table 1: Characteristics of different time series foundation models used for classification. For model size, our notations are the following: $\bullet \circ \circ$ is $<10\text{M}$ parameters, $\bullet \bullet \circ$ is in $[10\text{M}, 100\text{M}]$ and $\bullet \bullet \bullet$ is for models having more than 100M parameters.

Model name	Multivar Support	Zero-shot	HuggingFace Support	Model Size
Mantis	✓	✓	✓	$\bullet \circ \circ$
UniTS	✓	✗	✗	$\bullet \circ \circ$
NuTime	✓	✓	✗	$\bullet \circ \circ$
GPT4TS	✓	✗	✗	$\bullet \bullet \circ$
MOMENT	✗	✓	✓	$\bullet \bullet \bullet$

When it comes to quantifying the uncertainty of a fine-tuned foundation model, we consider its predicted probabilities $\sigma(h \circ F(\mathbf{x}))$, with $\sigma : \mathbb{R}^K \rightarrow \Delta_K$ being the softmax transformation that projects logits onto the probability simplex $\Delta_K = \{\mathbf{p} \in [0, 1]^K \mid \|\mathbf{p}\|_1 = 1\}$. We particularly focus on the top probability $\text{conf}(\mathbf{x}) = \max[\sigma(h \circ F(\mathbf{x}))]$, which we consider the confidence of the model in classifying \mathbf{x} . For the sake of simplicity, the predicted label we denoted by $\hat{y} = \text{argmax}[\sigma(h \circ F(\mathbf{x}))]$.

2.2 Data Pre-processing

Since time series data may vary in sequence lengths and units of measurement, pre-processing is required for both pre-training and inference. Similar to practices in computer vision, we pre-train the model with fixed input dimensions and resize inputs during inference and fine-tuning. Specifically, we set the input sequence length of Mantis to 512 and resize inputs using PyTorch’s interpolation function (Paszke et al., 2019). To address the issue of varying units of measurement, we apply instance-level standard scaling. For each time series observation (and, in the case of multiple channels, for each individual channel), we subtract the mean and divide by the standard deviation calculated across the time steps. This scaling process is implemented directly within the model architecture, ensuring that inputs are transformed during the forward pass.

2.3 Architecture

Below, we give details on the architecture of Mantis, which is an adaptation of the Vision Transformer (ViT, Dosovitskiy et al., 2021) to the time series framework. The entire architecture is depicted in Figure 1.

Token Generator Unit. The first step is to encode a time series into meaningful tokens, which are then passed to a transformer. Our token generation process consists of the following steps:

- Before encoding a time series, we perform instance-level normalization, as explained in Section 2.2. We then split the time series into patches. While Lin et al. (2024) and Nie et al. (2023) directly split the time series into non-overlapping and overlapping patches, respectively, we achieve this by applying a single convolution layer followed by mean pooling to obtain 32 patches. We set the number of output channels in the convolution to 256, which means each patch represents 256 convolutional features.
- Similarly, we generate patches for the time series differential, which is computed by taking the difference between two adjacent timestamps. The main idea behind the differential is to make the time series stationary, thus reducing the influence of trends. In Section 3.4, we show that incorporating this feature improves the overall performance.
- To preserve information about the original unit measurements, we split the raw time series observation (i.e., before instance normalization) into 32 non-overlapping patches, compute the mean and standard deviation for each patch, and encode them using the Multi-Scaled Scalar Encoder (Lin et al., 2024).
- Finally, we concatenate all features (from the time series, its differential, and the statistics) and pass them through a linear projector followed by a layer normalization step (Ba et al., 2016), generating the final 32 tokens with a dimension of 256.

ViT Unit. We then feed the generated tokens into a ViT unit, with the main steps summarized below:

- First, we append a class token to the 32 tokens generated in the previous step. As a learnable vector, the class token is introduced to attend to all the other tokens, aggregating information from the entire input into the embedding associated with it.
- To incorporate information about the positions of the tokens, we use the classical sinusoidal positional encoding (Vaswani et al., 2017). The position embeddings are summed with the input tokens and fed into a series of transformer layers.
- The transformer layer is identical to the one used by Dosovitskiy et al. (2021). We apply 6 transformer layers, each with multi-head attention consisting of 8 heads. During pre-training, we use a dropout rate of 10%.
- Finally, the class token’s representation generated by the transformer serves as the final output of the foundation model.

Projector and Prediction Head. To use the output of the foundation model, we append different layers depending on whether the model is in the pre-training or fine-tuning stage:

- Pre-training:* At this stage, we add a layer normalization step followed by a linear layer, which projects the embeddings for calculating their similarities.
- Fine-tuning:* At this stage, we add a classification head that maps the embeddings to class logits.

2.4 Pre-training

We pre-train Mantis in a self-supervised way using a contrastive learning approach that aims to train an encoder that outputs similar representations for two random augmentations of the same sample (positive pair) and dissimilar representations for augmentations of two different samples (negative pair). More formally, let \mathcal{T} be a considered space of transformations (augmentations) such that $\forall \phi \in \mathcal{T}, \mathbf{x} \in \mathcal{X}$ we have $\phi(\mathbf{x}) \in \mathcal{X}$. To measure the similarity of two embeddings, we first project the output of the foundation model $F(\mathbf{x})$ to a new dimension using a projector $g: \mathbb{R}^q \rightarrow \mathbb{R}^{q'}$ and then compute the cosine similarity between the two vectors defined as follows:

$$s_{\cos}(\mathbf{a}, \mathbf{b}) := \frac{\mathbf{a}^\top \mathbf{b}}{\|\mathbf{a}\| \cdot \|\mathbf{b}\|}, \quad \forall (\mathbf{a}, \mathbf{b}) \in \mathbb{R}^{2q'}$$

Given a batch $B = \{\mathbf{x}_i\}_{i=1}^b$, for each example \mathbf{x}_i , we sample two augmentation functions ϕ and ψ uniformly from \mathcal{T} , i.e., $\phi, \psi \sim \mathcal{U}(\mathcal{T})$, compute the pairwise similarities between all the examples in the following way:

$$\mathbf{s}_i(\phi, \psi) = [s_{\cos}(g \circ F \circ \phi(\mathbf{x}_i), g \circ F \circ \psi(\mathbf{x}_j))]_{j=1}^b \in \mathbb{R}^b.$$

Following Oord et al. (2018) as well as He et al. (2020) and denoting the cross-entropy error function by $l_{ce}: \mathbb{R}^b \times \{1, \dots, b\} \rightarrow \mathbb{R}$, we update the weights of F and g by minimizing the contrastive loss which we define as

$$\sum_{i=1}^b l_{ce} \left(\frac{\mathbf{s}_i(\phi, \psi)}{T}, i \right),$$

where $T \in (0, +\infty)$ is a temperature that we fixed to 0.1.

Regarding the choice of augmentation methods, we empirically tested several augmentation functions and found that their effectiveness is highly dataset-dependent, as they may distort a time series and cause the loss of important information. For our pre-training, we chose the RandomCropResize augmentation (Figure 2), which involves randomly cropping $c\%$ of a time series (with the condition that the remaining $(1-c)\%$ forms a contiguous window) and then resizing the cropped portion to the original sequence length. We applied relatively moderate distortions, varying the crop rate from 0% to 20%, preserving the main structure of a time series.

As a pre-training dataset, we use a union of various public datasets including UCR (Dau et al., 2019), UEA (Bagnall et al., 2018, all except EigenWorms and InsectWingbeat), ECG (Clifford et al., 2017), EMG (Goldberger et al., 2000), Epilepsy (Andrzejak et al., 2001), FD-A and FD-B (Lessmeier et al., 2016), Gesture (Liu et al., 2009), HAR (Anguita et al., 2013), SleepEEG (Kemp et al., 2000). We ensure that test sets used for evaluation in Section 3 are not part of the pre-training dataset. The total pre-training consists of 7 million time series examples. We pre-trained the model for 100 epochs with a batch size equal to 2048 on 4 NVIDIA Tesla V100-32GB GPUs.

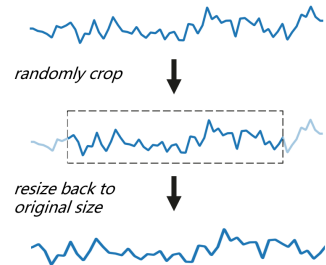


Figure 2: RandomCropResize

2.5 Adapters

Nowadays, the multivariate setting represents one of the main challenges for time series foundation models. In practice, different time series classification tasks vary in the number of channels, which raises non-trivial questions on how the model should be pre-trained and applied for a new task. Similarly to other foundation models (Goswami et al., 2024; Lin et al., 2024), Mantis is pre-trained in a univariate way and can be applied to the multivariate setting by treating each channel independently. However, this strategy has several limitations. Firstly, the foundation models are heavy by design, so treating all channels independently may lead to excessive resource consumption and failure to fine-tune them. Secondly, at the feature extraction step, the channel correlations are ignored, which may lead to the loss of some important information.

To address these concerns, we study a simple approach of using a channel-level adapter $a : \mathbb{R}^d \rightarrow \mathbb{R}^{d_{\text{new}}}$ that precedes the foundation model and transforms the original d channels into new d_{new} ones. While there are other ways to adapt foundation models to the multivariate setting (Zhang and Yan, 2023; Zhou et al., 2023), we consider this definition of an adapter due to its high flexibility: (a) not only Mantis but any foundation model can be plugged in, (b) channel-level transformation prevents from disrupting the temporal structure, (c) adaptation to the computation budget by determining the number of encoded channels.

In our experiments, we considered five adapters that we present further. Our idea was to test classical dimension reduction approaches like Principal Component Analysis (PCA) that are computationally efficient and are trained in an unsupervised way. However, their application is limited to 2D data matrices, making them not straightforward to use in our case. To overcome this problem, we train the dimension reduction method on the data reshaped to $(n \times t, d)$, where n is the number of training examples. Thus, with this trick, methods like PCA will be focused on correlations between channels over all time steps, capturing spatial correlations and learning the rotation matrix $W \in \mathbb{R}^{d_{\text{new}} \times d}$ that linearly combines the original channels into new ones. Overall, these four adapters rely on this strategy:

- *Principal Component Analysis (PCA)* seeks to find an orthogonal basis of principal components where few components capture most of the data variance.
- *Truncated Singular Value Decomposition (SVD, Halko et al., 2009)* is similar to PCA, but it applies SVD decomposition directly on the non-centered data matrix.
- *Random Projection (Rand Proj)* is a very simple baseline that projects data by randomly generating the rotation matrix $W \in \mathbb{R}^{d_{\text{new}} \times d}$.
- *Variance-Based Channel Selection (Var Selector)* is a feature selection method that selects channels with the highest variance. This approach can be useful when channels with low variance are not very informative, so they can be discarded without affecting the overall performance.

Although these adapters are computationally very efficient, they are not supervised meaning that they may lead to suboptimal classification performance. Following this reasoning, we introduce one more adapter:

- *Differentiable Linear Combiner (LComb)* performs a linear channel transformation $W \in \mathbb{R}^{D' \times D}$, which, unlike to previous adapters, is learned via backpropagation together with the encoder and classification head.

3 Experimental Results

In this section, we conduct a set of experiments to validate the high performance of our model. All our experiments have been performed on a single NVIDIA Tesla V100-32GB GPU.

3.1 Setup

Baselines. In our experiments, we compare Mantis with the State-of-the-Art (SOTA) time series classification foundation modeling. More specifically, these are the four following foundation models, whose implementation details can be found in Appendix A:

- UniTS (Gao et al., 2024) is a multi-task time series model that can be also considered as a foundation model with 1 million parameters. We use their checkpoint pre-trained in a supervised fashion on 18 datasets.
- GPT4TS (Zhou et al., 2023) is a method that partially fine-tunes a pre-trained GPT2 with an additional tokenization layer to perform different time series tasks including classification, anomaly detection, and forecasting. The total number of parameters is approximately 80 millions (10x larger than Mantis).

- NuTime (Lin et al., 2024) is a transformer-based TSFM for classification. Their pre-training dataset is very similar to the one we used, and the size of their model is smaller, containing approximately 2 million parameters.
- MOMENT (Goswami et al., 2024) is a TSFM based on the T5 architecture (Raffel et al., 2020) that has been pre-trained to cover different time series tasks including classification, anomaly detection, and forecasting. In total, MOMENT has 385 million parameters (approx. 48x larger than Mantis) and the pre-training dataset contained 1.13 billion samples.

Datasets. We use the following datasets to evaluate the performance of Mantis and compare it to other methods:

- UCR (Dau et al., 2019) that consists of 128 single-channel datasets.
- UEA (Bagnall et al., 2018) that has 30 multi-channel datasets. We exclude 3 datasets due to small test size or small sequence length, and subsample one dataset to ease computations (see more details in Appendix A). We further tag the remaining 27 datasets by UEA-27.
- 4 additional datasets used by Gao et al. (2024): Blink (Chicaiza and Benalcázar, 2021), MotionSenseHAR (Malekzadeh et al., 2019), EMOPain (Egede et al., 2020), SharePriceIncrease (Middlehurst et al., 2024).

Experiments. We have performed five different kinds of experiments, which we will briefly describe below. For all experiments except for the adapters, Mantis handles the multivariate case by sending all channels to the encoder independently.

1. *Zero-shot feature extraction.* In this experiment, we test the ability of Mantis to generate powerful embeddings without fine-tuning. For each downstream task, we extract features using the foundation model and then use them together with the training labels to learn a classifier. We use all considered datasets: the whole UCR collection, UEA-27, and 4 datasets from Gao et al. (2024), which results in 159 datasets (further denoted by 159-D).
2. *Fine-tuning with model selection.* For this experiment, we compare different foundation models when they are fine-tuned to a given downstream task. For each task, we use 80% of the original training set to fine-tune models and the rest 20% as a validation set to choose training hyperparameters. As we have fixed the batch size for all the considered methods, some methods did not fit a single GPU memory either due to the number of channels or the sequence length. This is why we removed from the results 15 datasets from UCR, 11 datasets from UEA, EMOPain, and MotionSenseHAR (see more details in Appendix A), so in total, we evaluate on 131 datasets (further tagged by 131-D).
3. *Ablation study.* In this experiment, we analyze the influence of different parts of the proposed methodology on the performance of Mantis. First, we show the advantage of extracting features from the time series’ differential for zero-shot extraction. Then, we analyze the influence of pre-training, fine-tuning, and model selection on the performance. We consider all the datasets except those with a large number of channels: 7 datasets from UEA and EMOPain. In total, it results in 151 datasets (further denoted by 151-D).
4. *Adapters.* We perform a comparative study of different adapters that extend Mantis to the large-dimensional case. In this experiment, consider all the UEA-27 datasets described before.
5. *Calibration.* Finally, we compare Mantis with other foundation models in terms of calibration of their predicted probabilities. We take the same experimental setup as for the *fine-tuning with model selection* experiment and, for each model, report the Expected Calibration Error (ECE, Naeini et al., 2015) before and after applying post-hoc calibration methods.

3.2 Comparison with SOTA: Zero-shot Feature Extraction

In this section, we use a time series foundation model as a feature extractor without fine-tuning it to a given downstream task. First, we generate embeddings for time series observations by passing them through the frozen encoder. Then, we use embeddings as new features to train a classifier and report its performance on test data. As a classifier, we have chosen the Random Forest algorithm (Breiman, 2001) due to its versatility and high performance without the need to perform hyperparameter searching. We fixed the number of trees to 200 while not restricting the maximum tree depth. In this section, we compare Mantis with NuTime and MOMENT while removing GPT4TS and UniTS from consideration as they have not provided a methodology for zero-shot extraction.

Figure 3 displays the performance results averaged over 159 datasets (159-D), while the complete results can be found in Appendix, Table 3. We can see that on average Mantis outperforms NuTime and MOMENT by 1.77% and 1.53%, respectively. Mantis is the best on 74 datasets, while MOMENT and NuTime have the best performance on 53 and 38 datasets, respectively. Compared to other foundation models, we can see that Mantis achieves the best balance in terms of the complexity of the model and its accuracy. On the one hand, Mantis outperforms a smaller model, NuTime, by increasing the encoder’s capacity and leveraging more information from the pre-training set. On the other hand, a much bigger model, MOMENT, with 385 million parameters does not manage to achieve a better performance despite its size.

In addition, comparing models in terms of running time, we notice that the forward pass of MOMENT is noticeably slower, which is especially pronounced with a large number of channels. To illustrate this observation, Figure 4 depicts the running time of Mantis and MOMENT on datasets from UEA-27. One can see that the inference time of MOMENT greatly increases with the dataset size.

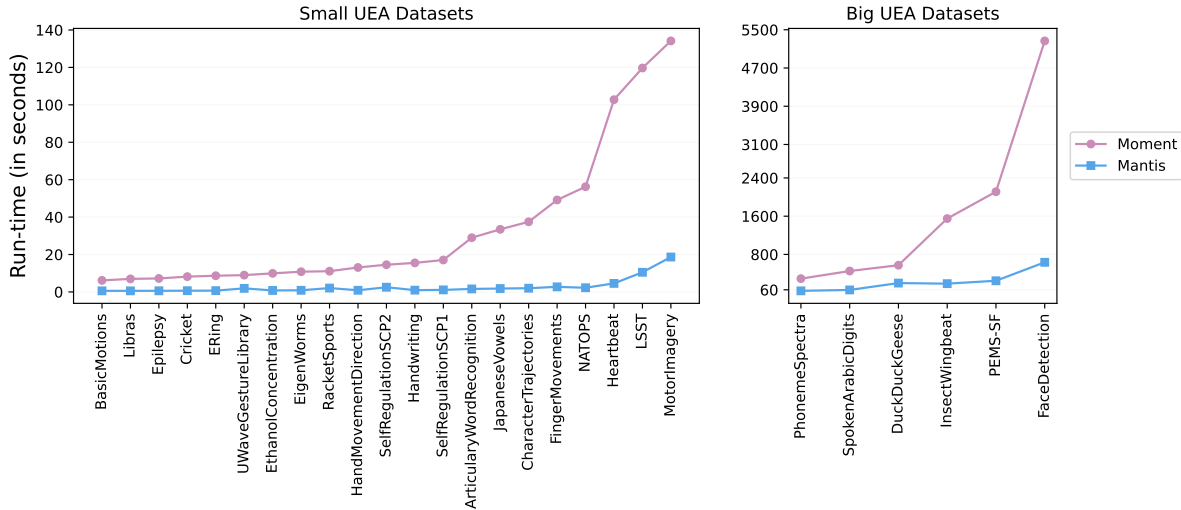


Figure 4: The running time of MOMENT and Mantis on the UEA-27 collection of datasets. For better visualization, we sort and split the datasets into two clusters based on the reported running time.

3.3 Comparison with SOTA: Fine-tuning

In this experiment, we perform a comparison by fine-tuning foundation models to a downstream task. More specifically, we append a prediction head after an encoder and fine-tune all layers or a subset of them on the training data. For all models under consideration, we fix a fine-tuning scheme: we minimize the cross-entropy loss for 100 epochs with a fixed batch size equal to 256, using an AdamW optimizer (Loshchilov et al., 2017) with a weight decay of 0.05. For each model and each dataset, We choose a learning rate over the grid: $\{10^{-4}, 2 \cdot 10^{-4}, 10^{-3}\}$ based on the validation set. For GPT4TS, we follow their paper and fine-tune the layers of the language backbone specified by the authors. For Mantis, NuTime, MOMENT, and UniTS, we perform fine-tuning of all the layers.

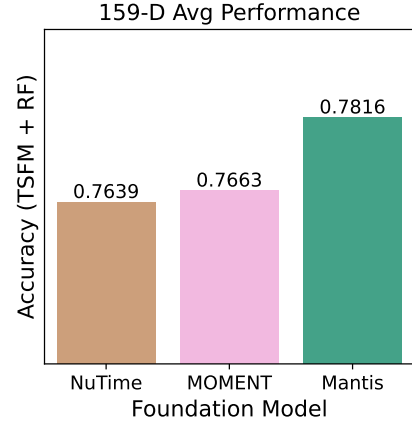


Figure 3: Zero-shot feature extraction: comparison with the SOTA. The accuracy is averaged over 3 random seeds and over 159-D datasets.

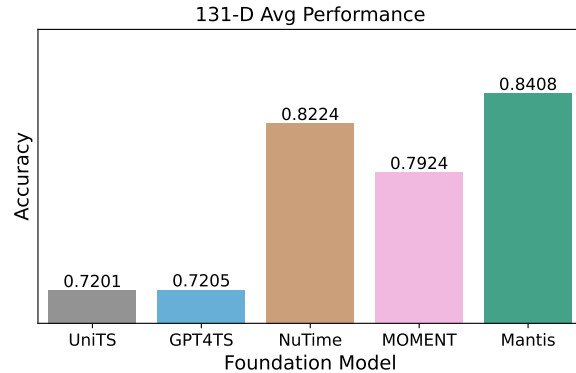


Figure 5: Model fine-tuning: comparison with the SOTA. The accuracy is averaged over 3 random seeds and over 131-D datasets.

In Figure 5, we illustrate the performance results averaged over 131 datasets (131-D). In Appendix, Table 4, we display the experimental results for every dataset. One can see that Mantis has the highest performance among all the considered foundation models. We note that the reported performance results of our competitors may diverge from those reported by the authors of these models. This may be explained by the difference in the chosen fine-tuning scheme. In our case, we have fixed the scheme for a fair comparison while trying to find the best learning rate for every model based on a validation set. Thus, our experimental results reveal that Mantis is the most robust to the choice of a fine-tuning scheme and does not necessarily require tedious hyperparameter searching. We additionally validate this argument in the next section by fine-tuning Mantis without any model selection.

3.4 Ablation Study

In this section, we perform several ablation experiments for a more thorough analysis of Mantis. First, we validate some of our architecture choices. More specifically, we test whether the incorporation of features extracted from the differential of a time series, proposed in Section 2.3, improves the quality of embeddings. For this, we have pre-trained another version of our foundation model where the differential feature extraction part was removed from the Token Generator Unit. In Figure 6, we plot the average zero-shot feature extraction performance of the two versions of Mantis, while the complete results may be found in Appendix, Table 5. One can see that the incorporation of the differential block noticeably improves the accuracy score. When comparing Figure 3 and Figure 6, it is interesting to notice that Mantis without the differential block still slightly outperforms NuTime and MOMENT in the case of zero-shot feature extraction.

In the second part of our ablation study, we raise the following questions: (a) is pre-training really useful, or it is sufficient to train Mantis from scratch on each dataset?, (b) should we fine-tune the head or the whole model?, (c) can Mantis be fine-tuned with default hyperparameters, and how much we can gain from the model selection? To answer these questions, we empirically compare the following fine-tuning regimes:

- The setup which we further call RF, and which we used for the zero-shot feature extraction experiment: the encoder of Mantis is frozen, and embeddings are used as features to train a Random Forest classifier.
- The encoder of Mantis is frozen, and the task is solved by fine-tuning a classification head, which, in our case, is layer normalization step + linear layer. The purpose of comparing this strategy, further called Head, with RF is to see the impact of the choice of a classifier (linear vs non-linear, differentiable vs non-differentiable) on the overall performance.
- The encoder is randomly initialized and fine-tuned together with a classification head. This baseline, which we further call Scratch, is introduced to see whether or not pre-training of Mantis is useful.
- Finally, the strategy further called Full consists in fine-tuning the pre-trained encoder together with a classification head.

In order to answer question (c), for every method, we report two scores: the test accuracy of the model at the last epoch (i.e., at the end of fine-tuning), and the best test accuracy of the model across all fine-tuning epochs. While the last epoch score gives a pessimistic evaluation of the performance as no model selection is performed, the best epoch score is an optimistic evaluation as it indicates the best achievable performance. In this experiment, we fix the fine-tuning scheme: the number of epochs is 100, the batch size is 256, the optimizer is AdamW with the weight decay of 0.05 and the learning rate set to $2 \cdot 10^{-4}$ and adjusted following the cosine annealing decay strategy (Loshchilov and Hutter, 2016) with 10 warm-up epochs.

Figure 7 depicts the average performance over the 151-D benchmark both for the last and best epoch, while the complete results can be found in Appendix, Table 6 and Table 7. First, we can see that the pre-training of Mantis is visibly useful as Full outperforms Scratch by 5.08% and 3.92% in the last and best epoch score, respectively. On the other hand, using a frozen pre-trained encoder is rather suboptimal in terms of performance, and full fine-tuning is preferred. This observation points out an important direction of future work, namely, to advance time series classification foundation models in terms of zero-shot performance.

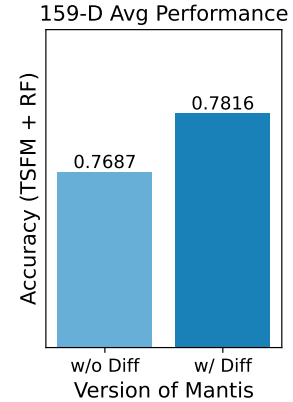


Figure 6: Mantis w/ and w/o the differential block. The accuracy is averaged over 3 random seeds and over 159-D datasets.

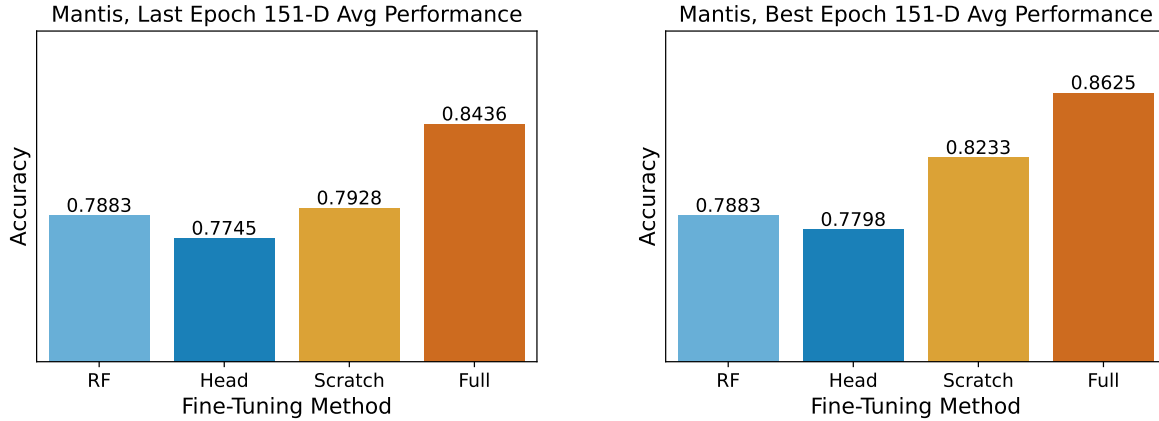


Figure 7: Performance of different fine-tuning methods for Mantis averaged over 3 random seeds and 151 datasets of the 151-D benchmark.

Another observation from Figure 7 is that fine-tuning the head with a frozen encoder may be suboptimal, and training a Random Forest on embeddings gives a slightly better accuracy score. Finally, by comparing the performance results for the last and best epoch, we conclude that although model selection is important to improve the overall performance (+1.89% for Full), using directly the model from the last epoch gives already good performance. This shows that Mantis can be applied in practice without the need to tediously search for optimal values of hyperparameters.

3.5 Adapters

In this section, we study the performance of Mantis when it is combined with one of the adapters we introduced in Section 2.5. For PCA, SVD, Rand Proj and Var Selector, the new number of channels is equal to $D' = \min\{D, 10\}$, while for LComb is always fixed to $D' = 10$. Table 2 depicts the empirical comparison between the adapters and the case when we treat all channels independently (dubbed as No Adapter). In addition, Figure 8 and Table 8 of the Appendix compare the no-fine-tuning case when Random Forest is used directly after the feature extraction step and the full fine-tuning with the best adapter chosen per dataset. Below, we discuss the experimental results.

Dimension reduction: When the number of channels is too large, the full fine-tuning of the foundation model is limited as treating all channels independently is computationally costly. In Table 2, one can see that starting from 28 channels and the batch size fixed to 256, the optimization of Mantis does not fit the memory of a single V100-32GB GPU card, which results in 7 NaN values in the No Adapter column. Nevertheless, applying one of the five adapters solves the issue, allowing the full fine-tuning and increasing the performance as can be seen in Table 8.

Channel interactions: Another advantage of adapters is that they mix the original channels allowing channels to interact before they are sent to the encoder. The utility of adapters from this perspective was shown by [Benechehab et al. \(2024\)](#) for zero-shot multivariate forecasting. Our experiments reveal that, in the classification context, conclusions are rather dataset-dependent: while for datasets like RacketSports and UWaveGestureLibrary, adapters do not bring any improvement compared No Adapter, transforming the original channels for datasets like Handwriting and HandMovementDirection, nevertheless, brings a large improvement.

Channel selection: In some cases certain channels do not contain any useful information, so they can simply be discarded. In such situations, the Var Selector has the highest performance, which we can observe on FingerMovements and InsectWingbeat datasets.

Differentiable adapter: Although on some datasets, LComb yields high performance, overall, its performance is lower than those of PCA, SVD and Var Selector. Since LComb is fine-tuned together with the encoder and the head, we suggest that the optimization of the adapter is intricate, so searching for a better optimization scheme can be a good direction for future work.

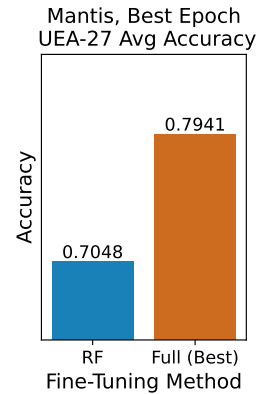


Figure 8: Mantis: zero-shot vs full fine-tuning with the best adapter per dataset.

Table 2: Performance comparison between different adapters when Mantis is fully-fine-tuned to a multi-channel time series classification task. The UEA-27 data collection is considered in this experiment, and the results are averaged over 3 random seeds. The number of selected channels is fixed to be ≤ 10 . No Adapter means that all channels are independently fed to the TSFM, and NaN in its performance results marks the cases when the model has not fitted to a single V100-32GB GPU card’s memory. Best Result summarizes the performance when the best strategy per dataset is chosen.

	d	No Adapter	Standalone Adapter				Diff. Adapter LComb	Best Result
			PCA	SVD	Rand Proj	Var Selector		
ArticulatoryWordRecognition	9	0.9933 ± 0.0	0.9922 ± 0.0019	0.9878 ± 0.0038	0.9811 ± 0.0038	0.9933 ± 0.0	0.9744 ± 0.0069	0.9933 ± 0.0
BasicMotions	6	1.0 ± 0.0	1.0 ± 0.0	1.0 ± 0.0	1.0 ± 0.0	1.0 ± 0.0	1.0 ± 0.0	1.0 ± 0.0
CharacterTrajectories	3	0.9928 ± 0.0004	0.9947 ± 0.0004	0.9923 ± 0.0012	0.9912 ± 0.0016	0.9928 ± 0.0004	0.993 ± 0.0018	0.9947 ± 0.0004
Cricket	6	1.0 ± 0.0	0.9861 ± 0.0	0.9769 ± 0.008	0.9722 ± 0.0	1.0 ± 0.0	0.9907 ± 0.008	1.0 ± 0.0
DuckDuckGeese	1345	NaN	0.5733 ± 0.0115	0.6 ± 0.02	0.54 ± 0.0872	0.5133 ± 0.0231	0.54 ± 0.0693	0.6 ± 0.02
ERing	4	0.9926 ± 0.0074	0.9778 ± 0.0064	0.9753 ± 0.0113	0.9642 ± 0.0043	0.9926 ± 0.0074	0.9778 ± 0.0064	0.9926 ± 0.0074
EigenWorms	6	0.8372 ± 0.0044	0.8448 ± 0.0117	0.8601 ± 0.0192	0.8117 ± 0.0233	0.8372 ± 0.0044	0.8066 ± 0.0384	0.8601 ± 0.0192
Epilepsy	3	1.0 ± 0.0	0.9976 ± 0.0042	0.9976 ± 0.0042	0.9976 ± 0.0042	1.0 ± 0.0	1.0 ± 0.0	1.0 ± 0.0
EthanolConcentration	3	0.4208 ± 0.0195	0.2928 ± 0.0101	0.3029 ± 0.0122	0.384 ± 0.0503	0.4208 ± 0.0195	0.4081 ± 0.0275	0.4208 ± 0.0195
FaceDetection	144	NaN	0.6026 ± 0.0054	0.6064 ± 0.0037	0.5638 ± 0.0065	0.5696 ± 0.0027	0.6272 ± 0.013	0.6272 ± 0.013
FingerMovements	28	NaN	0.5833 ± 0.0058	0.57 ± 0.06	0.5467 ± 0.0289	0.6167 ± 0.0058	0.58 ± 0.0265	0.6167 ± 0.0058
HandMovementDirection	10	0.4009 ± 0.0206	0.5135 ± 0.027	0.482 ± 0.0546	0.4279 ± 0.0512	0.4009 ± 0.0206	0.4414 ± 0.0624	0.5135 ± 0.027
Handwriting	3	0.482 ± 0.0157	0.4529 ± 0.0129	0.4588 ± 0.0224	0.4235 ± 0.0418	0.482 ± 0.0157	0.5839 ± 0.0283	0.5839 ± 0.0283
Heartbeat	61	NaN	0.7561 ± 0.0098	0.7626 ± 0.0123	0.7707 ± 0.0098	0.7951 ± 0.0129	0.774 ± 0.0123	0.7951 ± 0.0129
InsectWingbeatSubset	200	NaN	0.4703 ± 0.0051	0.4733 ± 0.0127	0.4803 ± 0.0302	0.591 ± 0.005	0.236 ± 0.0125	0.591 ± 0.005
JapaneseVowels	12	0.9811 ± 0.0054	0.9802 ± 0.0031	0.9811 ± 0.0	0.9577 ± 0.0271	0.9784 ± 0.0047	0.9577 ± 0.0128	0.9811 ± 0.0054
LSST	6	0.7109 ± 0.0015	0.6795 ± 0.0027	0.6894 ± 0.0021	0.6929 ± 0.0207	0.7109 ± 0.0015	0.6941 ± 0.0053	0.7109 ± 0.0015
Libras	2	0.9389 ± 0.0	0.937 ± 0.0032	0.9481 ± 0.0064	0.8111 ± 0.1392	0.9389 ± 0.0	0.9704 ± 0.0032	0.9704 ± 0.0032
MotorImagery	64	NaN	0.5933 ± 0.0351	0.5833 ± 0.0208	0.5867 ± 0.0379	0.6 ± 0.01	0.59 ± 0.0173	0.6 ± 0.01
NATOPS	24	0.937 ± 0.0116	0.9537 ± 0.0064	0.9611 ± 0.0	0.8926 ± 0.0032	0.8981 ± 0.0116	0.8796 ± 0.017	0.9611 ± 0.0
PEMS-SF	963	NaN	0.8536 ± 0.0067	0.8304 ± 0.0145	0.7457 ± 0.0473	0.9114 ± 0.0067	0.7476 ± 0.0219	0.9114 ± 0.0067
PhonemeSpectra	11	0.3421 ± 0.0023	0.3351 ± 0.009	0.3215 ± 0.0052	0.3492 ± 0.0033	0.344 ± 0.0052	0.3547 ± 0.0047	0.3547 ± 0.0047
RacketSports	6	0.9408 ± 0.0	0.9123 ± 0.0152	0.9101 ± 0.0076	0.9167 ± 0.0038	0.9408 ± 0.0	0.9254 ± 0.0038	0.9408 ± 0.0
SelfRegulationSCP1	6	0.9135 ± 0.0071	0.917 ± 0.0052	0.9113 ± 0.0034	0.9135 ± 0.0079	0.9135 ± 0.0071	0.901 ± 0.009	0.917 ± 0.0052
SelfRegulationSCP2	7	0.5389 ± 0.0096	0.5648 ± 0.0449	0.5685 ± 0.0251	0.5611 ± 0.0455	0.5389 ± 0.0096	0.5482 ± 0.021	0.5685 ± 0.0251
SpokenArabicDigits	13	0.987 ± 0.0009	0.9933 ± 0.0014	0.9906 ± 0.0019	0.988 ± 0.0027	0.9864 ± 0.0028	0.9882 ± 0.0016	0.9933 ± 0.0014
UWaveGestureLibrary	3	0.9438 ± 0.0108	0.8583 ± 0.0079	0.8552 ± 0.0095	0.8635 ± 0.0737	0.9438 ± 0.0108	0.9177 ± 0.0048	0.9438 ± 0.0108

3.6 Calibration

Uncertainty quantification is crucial when a learning model is part of a safety-critical system (Wang, 2023) or when its output is used to analyze the performance on test data (Xie et al., 2024). Consequently, in this section, we study the calibration properties of Mantis and other time series classification foundation models. We say a model is calibrated if, for a given confidence level α , the probability that the model predicts the true class is equal to α (Guo et al., 2017):

$$\mathbb{P}(Y = \hat{y} \mid \text{conf}(\mathbf{X}) = \alpha) = \alpha, \quad \forall \alpha \in [0, 1],$$

where \hat{y} and $\text{conf}(\mathbf{X})$ denote the predicted label and model’s confidence of a random variable \mathbf{X} , respectively, which were formally defined in Section 2.1. We consider the Expected Calibration Error (ECE, Naeini et al., 2015) as a metric to evaluate the calibration on a test set $\{\mathbf{x}_i, y_i\}_{i=1}^n$. We discretize the interval $[0, 1]$ into m disjoint bins: $B_j \cap B_k = \emptyset, \forall j \neq k, 1 \leq j, k \leq m$ and $\cup_{j=1}^m B_j = [0, 1]$. As commonly done in the literature, we split the interval into 10 equally spaced bins. Then, denoting the predicted label for \mathbf{x}_i by \hat{y}_i , the ECE is defined as follows:

$$\text{ECE} = \frac{1}{n} \sum_{j=1}^m \left| \sum_{\substack{1 \leq i \leq n \\ \text{conf}(\mathbf{x}_i) \in B_j}} \mathbb{I}(\hat{y}_i = y_i) - \text{conf}(\mathbf{x}_i) \right|.$$

Following the setup in Section 3.3, we evaluate the ECE before and after applying a *post-hoc* calibration for the five fine-tuned foundation models on 131 datasets from 131-D. We use two calibration techniques: (a) Temperature Scaling (Guo et al., 2017) that regulates the amplitude of logits before applying softmax, and (b) Isotonic Regression (Zadrozny and Elkan, 2002), a non-parametric method that adjusts predicted probabilities by fitting a piecewise constant function. For the second approach, instead of the classical algorithm, we consider the multi-class isotonic regression (IRM, Zhang et al., 2020) as it is shown to be less prone to overfitting. For each dataset, both approaches are fitted using the corresponding validation set (20% of training data as described in Section 3.1).

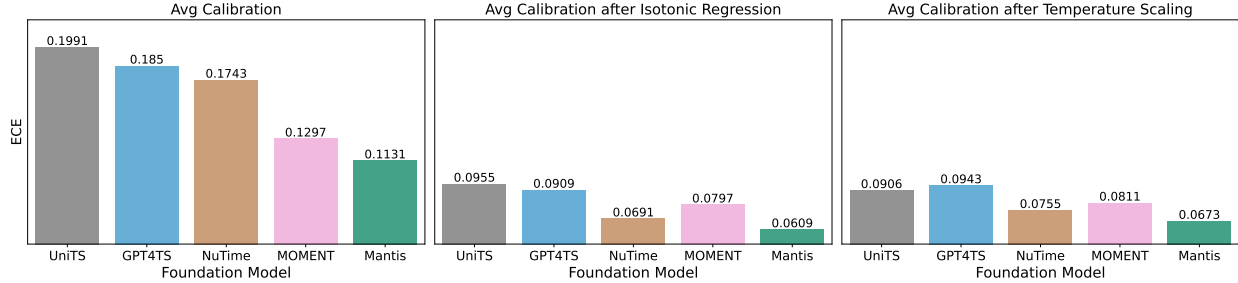


Figure 9: Averaged expected calibrated error of different methods over 131-D datasets.

In Figure 9, the Expected Calibration Error is displayed for the five foundation models under consideration before and after applying a post-hoc calibration method. We can observe that Mantis without any post-hoc calibration is the most calibrated model on average over 131 datasets, which is an important property for those applications where the number of training examples is not sufficient to construct a hold-out validation set. When posthoc calibration is applied, using either the Isotonic Regression or the Temperature Scaling, all foundation models become significantly better calibrated, yet Mantis remains the most calibrated.

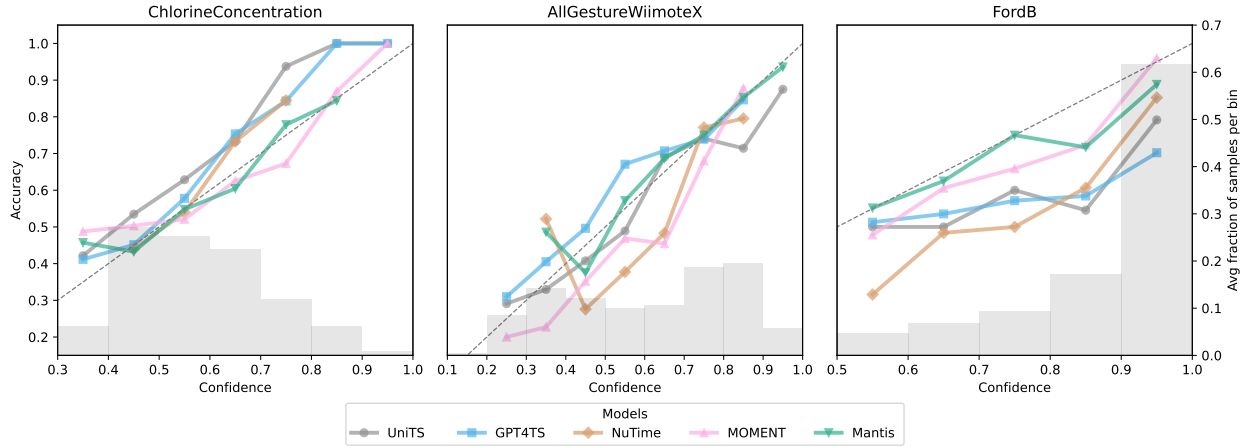


Figure 10: The reliability diagram on the test set after *post-hoc* temperature scaling on the validation set, for three different datasets. The gray histogram illustrates the distribution of the confidence score across the test set, where the chosen bins are identical to those used to evaluate the ECE.

4 Conclusion and Future Work

In this paper, we presented a technical report on Mantis, an [open-source](#), lightweight foundation model for time series classification. Our experimental results show that Mantis outperforms other foundation models while demonstrating superior calibration. We also introduced an adapter approach that offers a user-friendly solution for practitioners with limited computational resources. However, the results suggest that there is still much work to be done in advancing foundation models. First, we believe that designing foundation models for time series classification is a quite challenging task, as can be seen in Figure 11, where there is no clear correlation between model size and overall performance. Second, our results reveal a significant performance gap between the zero-shot feature extraction and full fine-tuning regimes, which indicates that there is still a big room for improvement. Finally, we believe that improving the interpretability of the model output is also an important direction for future work. Specifically, ensuring strong calibration properties of the foundation model could

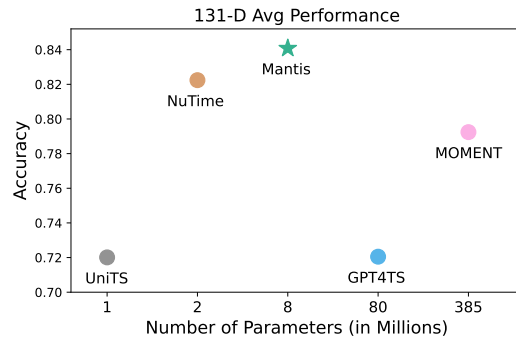


Figure 11: Accuracy vs Model Size.

enable various applications including uncertainty quantification and unsupervised performance prediction. In our earlier work (Wen et al., 2024), we also demonstrated that the hidden space itself can be performance-predictive when using contrastive pre-training. Thus, exploring Mantis from this perspective could be a promising direction for future work.

Acknowledgements

We would like to thank all the members of Paris Noah’s Ark Lab including Youssef Attia El Hili, Ambroise Odonnat, Abdelhakim Benechehab for their constructive comments that helped improve the manuscript.

References

- Achiam, J., Adler, S., Agarwal, S., Ahmad, L., Akkaya, I., Aleman, F. L., Almeida, D., Altenschmidt, J., Altman, S., Anadkat, S., et al. (2023). GPT-4 technical report. *arXiv preprint arXiv:2303.08774*.
- Andrzejak, R. G., Lehnertz, K., Mormann, F., Rieke, C., David, P., and Elger, C. E. (2001). Indications of nonlinear deterministic and finite-dimensional structures in time series of brain electrical activity: Dependence on recording region and brain state. *Physical Review E*, 64(6):061907.
- Anguita, D., Ghio, A., Oneto, L., Parra, X., Reyes-Ortiz, J. L., et al. (2013). A public domain dataset for human activity recognition using smartphones. In *Esann*, volume 3, page 3.
- Ansari, A. F., Stella, L., Turkmen, C., Zhang, X., Mercado, P., Shen, H., Shchur, O., Rangapuram, S. S., Arango, S. P., Kapoor, S., et al. (2024). Chronos: Learning the language of time series. *arXiv preprint arXiv:2403.07815*.
- Ba, J. L., Kiros, J. R., and Hinton, G. E. (2016). Layer normalization. *arXiv preprint arXiv:1607.06450*.
- Bagnall, A., Dau, H. A., Lines, J., Flynn, M., Large, J., Bostrom, A., Southam, P., and Keogh, E. (2018). The UEA multivariate time series classification archive, 2018. *arXiv preprint arXiv:1811.00075*.
- Benechehab, A., Hili, Y. A. E., Odonnat, A., Zekri, O., Thomas, A., Paolo, G., Filippone, M., Redko, I., and Kégl, B. (2024). Zero-shot model-based reinforcement learning using large language models. *arXiv preprint arXiv:2410.11711*.
- Bhethanabhotla, S. K., Swelam, O., Siems, J., Salinas, D., and Hutter, F. (2024). Mamba4Cast: Efficient zero-shot time series forecasting with state space models. *arXiv preprint arXiv:2410.09385*.
- Bommasani, R., Hudson, D. A., Adeli, E., Altman, R., Arora, S., von Arx, S., Bernstein, M. S., Bohg, J., Bosselut, A., Brunskill, E., et al. (2021). On the opportunities and risks of foundation models. *arXiv preprint arXiv:2108.07258*.
- Breiman, L. (2001). Random forests. *Machine learning*, 45:5–32.
- Cao, D., Jia, F., Arik, S. O., Pfister, T., Zheng, Y., Ye, W., and Liu, Y. (2023). TEMPO: Prompt-based generative pre-trained transformer for time series forecasting. *arXiv preprint arXiv:2310.04948*.
- Chang, C., Peng, W.-C., and Chen, T.-F. (2023). LLM4TS: Two-stage fine-tuning for time-series forecasting with pre-trained LLMs. *arXiv preprint arXiv:2308.08469*.
- Chicaiza, K. O. and Benalcázar, M. E. (2021). A brain-computer interface for controlling IoT devices using EEG signals. In *2021 IEEE Fifth Ecuador Technical Chapters Meeting (ETCM)*, pages 1–6. IEEE.
- Clifford, G. D., Liu, C., Moody, B., Li-wei, H. L., Silva, I., Li, Q., Johnson, A., and Mark, R. G. (2017). AF classification from a short single lead ECG recording: The PhysioNet/computing in cardiology challenge 2017. In *2017 Computing in Cardiology (CinC)*, pages 1–4. IEEE.
- Das, A., Kong, W., Sen, R., and Zhou, Y. (2023). A decoder-only foundation model for time-series forecasting. *arXiv preprint arXiv:2310.10688*.
- Dau, H. A., Bagnall, A., Kamgar, K., Yeh, C.-C. M., Zhu, Y., Gharghabi, S., Ratanamahatana, C. A., and Keogh, E. (2019). The UCR time series archive. *IEEE/CAA Journal of Automatica Sinica*, 6(6):1293–1305.
- Dempster, A., Petitjean, F., and Webb, G. I. (2020). ROCKET: exceptionally fast and accurate time series classification using random convolutional kernels. *Data Mining and Knowledge Discovery*, 34(5):1454–1495.
- Dosovitskiy, A., Beyer, L., Kolesnikov, A., Weissenborn, D., Zhai, X., Unterthiner, T., Dehghani, M., Minderer, M., Heigold, G., Gelly, S., Uszkoreit, J., and Houlsby, N. (2021). An image is worth 16x16 words: Transformers for image recognition at scale. *arXiv preprint arXiv:2010.11929*.

- Egede, J. O., Song, S., Olugbade, T. A., Wang, C., Amanda, C. D. C., Meng, H., Aung, M., Lane, N. D., Valstar, M., and Bianchi-Berthouze, N. (2020). Emopain challenge 2020: Multimodal pain evaluation from facial and bodily expressions. In *2020 15th IEEE International Conference on Automatic Face and Gesture Recognition (FG 2020)*, pages 849–856. IEEE.
- Eldele, E., Ragab, M., Chen, Z., Wu, M., Kwok, C. K., Li, X., and Guan, C. (2021). Time-series representation learning via temporal and contextual contrasting. In *Proceedings of the Thirtieth International Joint Conference on Artificial Intelligence, IJCAI-21*, pages 2352–2359.
- Gao, S., Koker, T., Queen, O., Hartvigsen, T., Tsiligkaridis, T., and Zitnik, M. (2024). UniTS: A unified multi-task time series model. In *The Thirty-eighth Annual Conference on Neural Information Processing Systems*.
- Goldberger, A. L., Amaral, L. A., Glass, L., Hausdorff, J. M., Ivanov, P. C., Mark, R. G., Mietus, J. E., Moody, G. B., Peng, C.-K., and Stanley, H. E. (2000). PhysioBank, PhysioToolkit, and PhysioNet: components of a new research resource for complex physiologic signals. *circulation*, 101(23):e215–e220.
- Goswami, M., Szafer, K., Choudhry, A., Cai, Y., Li, S., and Dubrawski, A. (2024). MOMENT: A family of open time-series foundation models. *arXiv preprint arXiv:2402.03885*.
- Gruver, N., Finzi, M., Qiu, S., and Wilson, A. G. (2024). Large language models are zero-shot time series forecasters. *Advances in Neural Information Processing Systems*, 36.
- Guo, C., Pleiss, G., Sun, Y., and Weinberger, K. Q. (2017). On calibration of modern neural networks. In *International conference on machine learning*, pages 1321–1330. PMLR.
- Halko, N., Martinsson, P.-G., and Tropp, J. A. (2009). Finding structure with randomness: Stochastic algorithms for constructing approximate matrix decompositions. *arXiv preprint arXiv:0909.4061*, 909.
- He, K., Fan, H., Wu, Y., Xie, S., and Girshick, R. (2020). Momentum contrast for unsupervised visual representation learning. In *Proceedings of the IEEE/CVF conference on computer vision and pattern recognition*, pages 9729–9738.
- He, K., Zhang, X., Ren, S., and Sun, J. (2015). Deep residual learning for image recognition. *arXiv preprint arXiv:1512.03385*.
- Ilbert, R., Odonnat, A., Feofanov, V., Virmaux, A., Paolo, G., Palpanas, T., and Redko, I. (2024). SAMformer: Unlocking the potential of transformers in time series forecasting with sharpness-aware minimization and channel-wise attention. In Salakhutdinov, R., Kolter, Z., Heller, K., Weller, A., Oliver, N., Scarlett, J., and Berkenkamp, F., editors, *Proceedings of the 41st International Conference on Machine Learning*, volume 235 of *Proceedings of Machine Learning Research*, pages 20924–20954. PMLR.
- Jin, M., Wang, S., Ma, L., Chu, Z., Zhang, J. Y., Shi, X., Chen, P.-Y., Liang, Y., Li, Y.-F., Pan, S., et al. (2023). Time-LLM: Time series forecasting by reprogramming large language models. *arXiv preprint arXiv:2310.01728*.
- Kemp, B., Zwinderman, A. H., Tuk, B., Kamphuisen, H. A., and Oberye, J. J. (2000). Analysis of a sleep-dependent neuronal feedback loop: the slow-wave microcontinuity of the EEG. *IEEE Transactions on Biomedical Engineering*, 47(9):1185–1194.
- Lessmeier, C., Kimotho, J. K., Zimmer, D., and Sextro, W. (2016). Condition monitoring of bearing damage in electromechanical drive systems by using motor current signals of electric motors: A benchmark data set for data-driven classification. *PHM Society European Conference*, 3(1).
- Lin, C., Wen, X., Cao, W., Huang, C., Bian, J., Lin, S., and Wu, Z. (2024). NuTime: Numerically multi-scaled embedding for large-scale time-series pretraining. *Transactions on Machine Learning Research*.
- Liu, J., Zhong, L., Wickramasuriya, J., and Vasudevan, V. (2009). uWave: Accelerometer-based personalized gesture recognition and its applications. *Pervasive and Mobile Computing*, 5(6):657–675.
- Loshchilov, I. and Hutter, F. (2016). SGDR: Stochastic gradient descent with warm restarts. In *International Conference on Learning Representations*.
- Loshchilov, I., Hutter, F., et al. (2017). Fixing weight decay regularization in Adam. *arXiv preprint arXiv:1711.05101*, 5.
- Malekzadeh, M., Clegg, R. G., Cavallaro, A., and Haddadi, H. (2019). Mobile sensor data anonymization. In *Proceedings of the international conference on internet of things design and implementation*, pages 49–58.
- Middlehurst, M., Schäfer, P., and Bagnall, A. (2024). Bake off redux: a review and experimental evaluation of recent time series classification algorithms. *Data Mining and Knowledge Discovery*, pages 1–74.
- Naeini, M. P., Cooper, G., and Hauskrecht, M. (2015). Obtaining well calibrated probabilities using Bayesian binning. *Proceedings of the AAAI conference on artificial intelligence*, 29(1).

- Nie, Y., H. Nguyen, N., Sinthong, P., and Kalagnanam, J. (2023). A time series is worth 64 words: Long-term forecasting with transformers. In *International Conference on Learning Representations*.
- Oord, A. v. d., Li, Y., and Vinyals, O. (2018). Representation learning with contrastive predictive coding. *arXiv preprint arXiv:1807.03748*.
- Paszke, A., Gross, S., Massa, F., Lerer, A., Bradbury, J., Chanan, G., Killeen, T., Lin, Z., Gimelshein, N., Antiga, L., et al. (2019). PyTorch: An imperative style, high-performance deep learning library. *Advances in neural information processing systems*, 32.
- Raffel, C., Shazeer, N., Roberts, A., Lee, K., Narang, S., Matena, M., Zhou, Y., Li, W., and Liu, P. J. (2020). Exploring the limits of transfer learning with a unified text-to-text transformer. *Journal of machine learning research*, 21(140):1–67.
- Rasul, K., Ashok, A., Williams, A. R., Khorasani, A., Adamopoulos, G., Bhagwatkar, R., Biloš, M., Ghonia, H., Hassen, N., Schneider, A., et al. (2023). Lag-llama: Towards foundation models for time series forecasting. In *RO-FoMo: Robustness of Few-shot and Zero-shot Learning in Large Foundation Models*.
- Touvron, H., Lavril, T., Izacard, G., Martinet, X., Lachaux, M.-A., Lacroix, T., Rozière, B., Goyal, N., Hambro, E., Azhar, F., et al. (2023). Llama: Open and efficient foundation language models. *arXiv preprint arXiv:2302.13971*.
- Vaswani, A., Shazeer, N., Parmar, N., Uszkoreit, J., Jones, L., Gomez, A. N., Kaiser, L. u., and Polosukhin, I. (2017). Attention is all you need. In Guyon, I., Luxburg, U. V., Bengio, S., Wallach, H., Fergus, R., Vishwanathan, S., and Garnett, R., editors, *Advances in Neural Information Processing Systems*, volume 30. Curran Associates, Inc.
- Wang, C. (2023). Calibration in deep learning: A survey of the state-of-the-art. *arXiv preprint arXiv:2308.01222*.
- Wang, Y., Qiu, Y., Chen, P., Zhao, K., Shu, Y., Rao, Z., Pan, L., Yang, B., and Guo, C. (2024). ROSE: Register assisted general time series forecasting with decomposed frequency learning. *arXiv preprint arXiv:2405.17478*.
- Wei, W. W. (2018). *Multivariate time series analysis and applications*. John Wiley & Sons.
- Wen, S., Feofanov, V., and Zhang, J. (2024). Measuring pre-training data quality without labels for time series foundation models. *arXiv preprint arXiv:2412.06368*.
- Woo, G., Liu, C., Kumar, A., Xiong, C., Savarese, S., and Sahoo, D. (2024). Unified training of universal time series forecasting transformers. In Salakhutdinov, R., Kolter, Z., Heller, K., Weller, A., Oliver, N., Scarlett, J., and Berkenkamp, F., editors, *Proceedings of the 41st International Conference on Machine Learning*, volume 235 of *Proceedings of Machine Learning Research*, pages 53140–53164. PMLR.
- Xie, R., Odonnat, A., Feofanov, V., Deng, W., Zhang, J., and An, B. (2024). MANO: Exploiting matrix norm for unsupervised accuracy estimation under distribution shifts. *arXiv preprint arXiv:2405.18979*.
- Xue, H. and Salim, F. D. (2023). Promptcast: A new prompt-based learning paradigm for time series forecasting. *IEEE Transactions on Knowledge and Data Engineering*.
- Yue, Z., Wang, Y., Duan, J., Yang, T., Huang, C., Tong, Y., and Xu, B. (2022). TS2Vec: Towards universal representation of time series. *Proceedings of the AAAI Conference on Artificial Intelligence*, 36(8):8980–8987.
- Zadrozny, B. and Elkan, C. (2002). Transforming classifier scores into accurate multiclass probability estimates. In *Proceedings of the eighth ACM SIGKDD international conference on Knowledge discovery and data mining*, pages 694–699.
- Zhang, J., Kailkhura, B., and Han, T. Y.-J. (2020). Mix-n-Match: Ensemble and compositional methods for uncertainty calibration in deep learning. In *International conference on machine learning*, pages 11117–11128. PMLR.
- Zhang, X., Zhao, Z., Tsiligkaridis, T., and Zitnik, M. (2022). Self-supervised contrastive pre-training for time series via time-frequency consistency. In Koyejo, S., Mohamed, S., Agarwal, A., Belgrave, D., Cho, K., and Oh, A., editors, *Advances in Neural Information Processing Systems*, volume 35, pages 3988–4003. Curran Associates, Inc.
- Zhang, Y. and Yan, J. (2023). Crossformer: Transformer utilizing cross-dimension dependency for multivariate time series forecasting. In *The eleventh international conference on learning representations*.
- Zhou, T., Niu, P., Sun, L., Jin, R., et al. (2023). One fits all: Power general time series analysis by pretrained LM. *Advances in neural information processing systems*, 36:43322–43355.

A Experimental Setup

A.1 Datasets and Benchmarks

Below we give more details how datasets were chosen for each benchmark.

- *UCR*: For some datasets, the sequences are very long, so fine-tuning GPT4TS does not fit the memory. These are the following 15 datasets: EOGHorizontalSignal, EOGVerticalSignal, EthanolLevel, HandOutlines, InlineSkate, MixedShapesRegularTrain, PLAID, PigAirwayPressure, PigArtPressure, PigCVP, SemgHandGenderCh2, SemgHandMovementCh2, SemgHandSubjectCh2, StarLightCurves, and UWaveGestureLibraryAll.
- *UEA*: We have excluded AtrialFibrillation and StandWalkJump datasets due to their very small test size and PenDigits due to its very small sequence length. For InsectWingbeat dataset, we subsampled 1000 examples from the original training set (which contains 30,000 examples) and 1000 from the original test set (of 20,000 examples) to reduce computational overhead while maintaining sufficient variety in the data for robust model evaluation. The following 7 datasets have a very large number of channels, creating issues with full fine-tuning: DuckDuckGeese, FaceDetection, FingerMovements, Heartbeat, InsectWingbeat, MotorImagery, and PEMS-SF. In addition, GPT4TS failed to handle long sequences of the following 4 datasets: EigenWorms, EthanolConcentration, SelfRegulationSCP1, and SelfRegulationSCP2.
- *Other datasets*: EMOPain has a lot of channels making the full fine-tuning costly, while MotionSenseHAR has too long sequences for GPT4TS.

To sum up, for Section 3.2 and the first experiment of Section 3.4, we use all 159 datasets without exceptions; for Section 3.3 and Section 3.6, we exclude all long and high-dimensional datasets, i.e., 15 datasets from UCR, 7+4 datasets from UEA, 2 datasets from the others; for the second experiment of Section 3.4, we exclude only high-dimensional datasets, i.e., 7 datasets from UEA + EMOPain dataset; finally, for Section 3.5, we use all 27 UEA datasets under consideration.

A.2 Implementation Details

- *MOMENT*: We use the MOMENT-large model (`d_model=1024`), which pre-trained weights can be found on the corresponding [HuggingFace](#) repository. To handle the multi-channel setup, we process every channel independently and concatenate all the embeddings before passing them to the classification head. In the paper, they have considered datasets with a sequence length ≤ 512 and use zero-padding to fix the input size to 512. At the same time, we have also tried to interpolate sequences to 512 instead, and it did not affect the performance of MOMENT. Thus, we have decided to stick to the latter option as it allows us to evaluate MOMENT for any sequence length.
- *GPT4TS*: We use the `code` provided by the authors. As a backbone, the model uses 6 layers from the pre-trained GPT2, which checkpoint can be found on [HuggingFace](#). Channels are processed simultaneously as a part of their tokenizer. Stride and patch size are fixed to 8.
- *NuTime*. We use the pre-trained weights provided by the authors in their [GitHub](#) repository, while fixing the hyperparameters of the architecture according to [this](#) configuration file. In contrast to the original implementation, we do not use their adapter (described in Section 3.4 of their paper) but process all channels independently as for Mantis and MOMENT. This allows us to use NuTime in the zero-shot feature extraction setting as their adapter has to be fine-tuned.
- *UniTS*. We use the implementation and the checkpoint provided the authors at their [GitHub](#) repository. Similarly to Mantis, MOMENT and NuTime, channels are processed independently. Stride and patch size are set to 16. Dimension of the model is 64.

B Complete Results

Below we provide full tables with experimental results.

Table 3: Comparison of 3 TSFMs under the feature extraction regime on the 159-D benchmark. The performance is averaged over 3 random seeds and reported with the standard deviation.

	NuTime	MOMENT	Mantis		NuTime	MOMENT	Mantis
ACSF1	0.7367±0.0351	0.75 ±0.0173	0.6133±0.0208	ItalyPowerDemand	0.8698±0.007	0.9498 ±0.0006	0.9077±0.0035
Adiac	0.7255±0.0115	0.7886 ±0.0074	0.7332±0.0039	LargeKitchenAppliances	0.7227±0.0027	0.7333±0.0071	0.7804 ±0.0041
AllGestureWiimoteX	0.661±0.003	0.6105±0.0136	0.6705 ±0.0044	Lightning2	0.6885±0.0164	0.7377±0.0328	0.8033 ±0.0
AllGestureWiimoteY	0.6362±0.0079	0.6576±0.0079	0.6671 ±0.0057	Lightning7	0.6895±0.0158	0.6758±0.0209	0.7763 ±0.0285
AllGestureWiimoteZ	0.6024±0.0179	0.5767±0.0103	0.6695 ±0.0033	Mallat	0.8304±0.0025	0.859±0.0111	0.8903 ±0.0137
ArrowHead	0.76±0.0198	0.8076 ±0.0144	0.7105±0.0175	Meat	0.8889±0.0192	0.9444 ±0.0096	0.9389±0.0096
BME	0.8444±0.0168	0.9756 ±0.0139	0.9311±0.0038	MedicalImages	0.7044±0.0027	0.6939±0.0062	0.7079 ±0.0035
Beef	0.6556±0.077	0.7444 ±0.0509	0.6556±0.0509	MelbournePedestrian	0.912 ±0.0045	0.8662±0.0047	0.9016±0.0031
BeetleFly	0.8667±0.0289	0.95 ±0.0	0.85±0.05	MiddlePhalanxOutlineAgeGroup	0.6169 ±0.0065	0.5779±0.0065	0.5801±0.0099
BirdChicken	0.9667±0.0289	0.85±0.0	1.0 ±0.0	MiddlePhalanxOutlineCorrect	0.7858±0.0099	0.8625 ±0.006	0.8099±0.0099
CBF	0.9744±0.0011	0.9411±0.0078	0.993 ±0.0013	MiddlePhalanxTW	0.5238±0.0037	0.5952 ±0.0037	0.5368±0.0099
Car	0.75±0.0	0.7944 ±0.0255	0.7722±0.0419	MixedShapesRegularTrain	0.9392±0.0013	0.9124±0.0023	0.943 ±0.0044
Chinatown	0.932±0.0017	0.9806 ±0.0034	0.8737±0.0168	MixedShapesSmallTrain	0.9061 ±0.0029	0.8389±0.0041	0.8961±0.0004
ChlorineConcentration	0.6675±0.0035	0.6901 ±0.0042	0.6806±0.0019	MoteStrain	0.9462 ±0.0032	0.8914±0.0083	0.9137±0.0136
CinCECGTorso	0.737 ±0.0152	0.6998±0.0118	0.6611±0.0036	NonInvasiveFetalECGThorax1	0.7696±0.0049	0.8887 ±0.0035	0.6222±0.0037
Coffee	0.9167±0.0206	0.8929±0.0	0.9524 ±0.0206	NonInvasiveFetalECGThorax2	0.811±0.0016	0.9138 ±0.0006	0.6872±0.0025
Computers	0.78 ±0.004	0.6173±0.0162	0.7373±0.0092	OSULeaf	0.7975±0.0072	0.7355±0.0041	0.8747 ±0.0104
CricketX	0.6701±0.0146	0.6795±0.0051	0.7368 ±0.0171	OliveOil	0.7111±0.0192	0.9±0.0	0.9333 ±0.0
CricketY	0.6556±0.0053	0.6897±0.0077	0.7504 ±0.0065	PLAID	0.7933±0.0113	0.7312±0.0088	0.8181 ±0.0047
CricketZ	0.6863±0.0171	0.7128±0.0044	0.7906 ±0.0039	PhalangesOutlinesCorrect	0.7743±0.0041	0.8248 ±0.0007	0.7786±0.0042
Crop	0.6683±0.0026	0.7035 ±0.0026	0.6756±0.0018	Phoneme	0.2802±0.0044	0.2751±0.0062	0.323 ±0.0034
DiatomSizeReduction	0.8322±0.0115	0.8867 ±0.0019	0.8845±0.0019	PickupGestureWiimoteZ	0.6933±0.0808	0.68±0.06	0.74 ±0.02
DistalPhalanxOutlineAgeGroup	0.7362±0.011	0.7506±0.011	0.789 ±0.015	PigAirwayPressure	0.3782±0.01	0.1186±0.0028	0.484 ±0.0147
DistalPhalanxOutlineCorrect	0.7742±0.0055	0.7886 ±0.0055	0.75±0.0126	PigArtPressure	0.9391 ±0.0028	0.6106±0.0048	0.9103±0.0028
DistalPhalanxTW	0.6763±0.0	0.6571±0.011	0.6859 ±0.011	PigCVP	0.8381 ±0.0242	0.609±0.0373	0.7837±0.0127
DodgerLoopDay	0.5167±0.0361	0.4542±0.0144	0.55 ±0.0217	Plane	0.9937±0.0055	0.9841±0.0145	1.0 ±0.0
DodgerLoopGame	0.756±0.0084	0.8116 ±0.0126	0.7585±0.0221	PowerCons	0.9352±0.0032	0.9463 ±0.0032	0.9093±0.0032
DodgerLoopWeekend	0.9565±0.0072	0.9614 ±0.0111	0.9517±0.0084	ProximalPhalanxOutlineAgeGroup	0.8537 ±0.0049	0.839±0.0049	0.8537 ±0.0049
ECG200	0.8133±0.0153	0.8967 ±0.0153	0.82±0.01	ProximalPhalanxOutlineCorrect	0.8385±0.0034	0.8751 ±0.0052	0.8202±0.0086
ECG5000	0.9313±0.0003	0.9384 ±0.0008	0.9211±0.001	ProximalPhalanxTW	0.8065±0.0056	0.8114 ±0.0028	0.7691±0.0028
ECGFiveDays	0.7801±0.017	0.8564±0.0223	0.909 ±0.0218	RefrigerationDevices	0.5564 ±0.0041	0.536±0.0046	0.504±0.0122
EOGHorizontalSignal	0.4346±0.0032	0.5571±0.0112	0.5875 ±0.0089	Rock	0.6067±0.0306	0.84 ±0.02	0.7133±0.0115
EOGVerticalSignal	0.2716±0.008	0.4595±0.0097	0.4751 ±0.0	ScreenType	0.5324 ±0.0077	0.4436±0.0178	0.4649±0.0134
Earthquakes	0.7458±0.0042	0.7458±0.0042	0.7482 ±0.0	SemgHandGenderCh2	0.8928±0.0042	0.8028±0.0079	0.9189 ±0.0086
ElectricDevices	0.7046±0.0014	0.7142±0.001	0.7226 ±0.0026	SemgHandMovementCh2	0.72±0.0038	0.5237±0.0013	0.797 ±0.0056
EthanolLevel	0.3407±0.0101	0.4227 ±0.0058	0.2993±0.011	SemgHandSubjectCh2	0.7741±0.0134	0.6815±0.0026	0.8622 ±0.0135
FaceAll	0.6363±0.0053	0.7398±0.0074	0.7815 ±0.0074	ShakeGestureWiimoteZ	0.9267 ±0.0115	0.8533±0.0115	0.8867±0.0115
FaceFour	0.7841±0.0521	0.7765±0.0174	0.9508 ±0.0066	ShapeletSim	0.8833±0.0111	0.9648 ±0.0064	0.9278±0.0111
FacesUCR	0.7141±0.003	0.7951±0.0034	0.8354 ±0.0054	ShapesAll	0.8194±0.0025	0.8239 ±0.0092	0.8194±0.0054
FiftyWords	0.5949±0.0125	0.6777 ±0.0111	0.6462±0.0096	SmallKitchenAppliances	0.8027±0.0071	0.72±0.0141	0.8089 ±0.0081
Fish	0.9162±0.0033	0.8705±0.0201	0.9333 ±0.0066	SmoothSubspace	0.8933±0.0067	0.92 ±0.0133	0.9067±0.0115
FordA	0.8932±0.002	0.9015 ±0.0008	0.8581±0.0048	SonyAIBORobotSurface1	0.7987±0.0044	0.8087 ±0.006	0.787±0.0294
FordB	0.7642±0.0119	0.765 ±0.0019	0.7305±0.0031	SonyAIBORobotSurface2	0.8297±0.0034	0.8353±0.0106	0.8552 ±0.0168
FreezerRegularTrain	0.9738 ±0.0013	0.8994±0.0012	0.9374±0.0043	StarLightCurves	0.9792 ±0.0002	0.9734±0.0004	0.9759±0.0005
FreezerSmallTrain	0.9549 ±0.0059	0.7758±0.0067	0.7942±0.0059	Strawberry	0.9378±0.0072	0.9604 ±0.0016	0.9514±0.0027
Fungi	0.7043±0.0093	0.9964 ±0.0062	0.8262±0.0164	SwedishLeaf	0.9205±0.0065	0.9205±0.0051	0.9275 ±0.0009
GestureMidAirD1	0.6744 ±0.0379	0.6744 ±0.0044	0.659±0.0044	Symbols	0.9407±0.0126	0.938±0.0126	0.968 ±0.0056
GestureMidAirD2	0.5692±0.0	0.5744±0.016	0.6154 ±0.0077	SyntheticControl	0.9667±0.0033	0.9433±0.0	0.9767 ±0.0067
GestureMidAirD3	0.3974 ±0.0247	0.359±0.0118	0.3282±0.016	ToeSegmentation1	0.8596±0.0044	0.924±0.0127	0.9635 ±0.0067
GesturePebbleZ1	0.8915±0.0067	0.8469±0.0067	0.9283 ±0.0034	ToeSegmentation2	0.7256±0.016	0.8462±0.0077	0.9282 ±0.0044
GesturePebbleZ2	0.8165±0.011	0.8376±0.0073	0.9219 ±0.0256	Trace	1.0 ±0.0	0.99±0.0	1.0 ±0.0
GunPoint	0.9444±0.0038	1.0 ±0.0	0.98±0.0067	TwoLeadECG	0.8712±0.0303	0.9649±0.0116	0.9962 ±0.0005
GunPointAgeSpan	0.9684±0.0032	0.962±0.0032	0.9905 ±0.0	TwoPatterns	0.8414±0.0041	0.8919 ±0.0079	0.8802±0.0079
GunPointMaleVersusFemale	0.962±0.0032	0.9884±0.0018	0.9958 ±0.0018	UMD	0.9329±0.0223	0.9699±0.004	0.9722 ±0.0069
GunPointOldVersusYoung	1.0 ±0.0	0.9577±0.008	0.9968±0.0	UWaveGestureLibraryAll	0.8773±0.0028	0.8975 ±0.0021	0.8458±0.0057
Ham	0.7206±0.022	0.7714 ±0.0	0.673±0.0145	UWaveGestureLibraryX	0.8053 ±0.0007	0.7829±0.0071	0.7696±0.0028
HandOutlines	0.9045±0.0062	0.909±0.0056	0.9162 ±0.0072	UWaveGestureLibraryY	0.7338 ±0.0032	0.7022±0.0026	0.6874±0.0022
Haptics	0.4481±0.0056	0.5152 ±0.0068	0.4968±0.0032	UWaveGestureLibraryZ	0.7427 ±0.0036	0.73±0.002	0.7324±0.0036
Herring	0.599±0.0325	0.6146±0.009	0.6667 ±0.0239	Wafer	0.9933 ±0.0006	0.9867±0.0003	0.9903±0.0003
HouseTwenty	0.8655±0.0084	0.9356±0.0097	0.9412 ±0.0	Wine	0.7469±0.0107	0.8457 ±0.0283	0.7901±0.0107
InlineSkate	0.357±0.0105	0.3176±0.001	0.363 ±0.0136	WordSynonyms	0.5199±0.0127	0.6003 ±0.0078	0.5502±0.0081
InsectEPGRegularTrain	1.0 ±0.0	0.9183±0.0061	1.0 ±0.0	Worms	0.7403 ±0.0	0.7056±0.015	0.6537±0.027
InsectEPGSmallTrain	1.0 ±0.0	0.8501±0.0061	1.0 ±0.0	WormsTwoClass	0.7835±0.0075	0.7706 ±0.0075	0.8139 ±0.0198
InsectWingbeatSound	0.5066±0.0066	0.6158 ±0.0037	0.519±0.0044	Yoga	0.8219±0.0015	0.8264 ±0.003	0.815±0.0012
Blink	0.6926±0.0156	0.9911±0.0022	0.9993 ±0.0013	Handwriting	0.2035±0.0082	0.236±0.005	0.339 ±0.01
EMOPain	0.8836 ±0.0016	0.8432±0.0091	0.8385±0.0016	Heartbeat	0.7756±0.0	0.727±0.005	0.798 ±0.017
MotionSenseHAR	0.9887±0.0	0.9673±0.0022	0.9975 ±0.0022	InsectWingbeatSubset	0.611 ±0.0066	0.243±0.011	0.607±0.007
SharePriceIncrease	0.6932 ±0.0006	0.6832±0.0082	0.6833±0.0049	JapaneseVowels	0.9405±0.0072	0.88±0.009	0.963 ±0.006
ArticulatoryWordRecognition	0.9933 ±0.0	0.98±0.0	0.993±0.003	LSSST	0.5668±0.0068	0.621 ±0.001	0.605±0.002
BasicMotions	1.0 ±0.0	0.992±0.014	1.0 ±0.0	Libras	0.8852±0.0064	0.85±0.02	0.898 ±0.008
CharacterTrajectories	0.9649±0.0038	0.97 ±0.002	0.94±0.001	MotorImagery	0.5367±0.0153	0.547±0.055	0.55 ±0.036
Cricket	0.9907±0.008	0.977±0.008	1.0 ±0.0	NATOPS	0.8426±0.014	0.822±0.024	0.907 ±0.013
DuckDuckGeese	0.4267±0.0503	0.433 ±0.031	0.407±0.031	PEMS-SF	0.9884±0.0	1.0 ±0.0	0.985±0.013
ERing	0.9716 ±0.0057	0.969±0.008	0.941±0.01	PhonemeSpectra	0.2588±0.0065	0.215±0.001	0.273 ±0.008
EigenWorms	0.7786 ±0.0202	0.735±0.016	0.753±0.016	RacketSports	0.9101±0.01	0.82±0.01	0.923 ±0.004
Epilepsy	1.0 ±0.0	0.988±0.004	0.995±0.004	SelfRegulationSCP1	0.7702±0.012	0.754±0.012	0.804 ±0.011
EthanolConcentration	0.3942 ±0.0158	0.278±0.008	0.27±0.01	SelfRegulationSCP2	0.5 ±0.0242	0.496±0.002	0.476±0.045
FaceDetection	0.5581 ±0.0077	0.544±0.011	0.526±0.002	SpokenArabicDigits	0.8968±0.0032	0.935 ±0.002	0.839±0.005
FingerMovements	0.5133±0.0153	0.497±0.023	0.54 ±0.035	UWaveGestureLibrary	0.8792 ±0.0018	0.873±0.011	0.814±0.01
HandMovementDirection	0.3108±0.0234	0.315 ±0.008	0.212±0.041	Best Count	38	53	74

Table 4: Comparison of different SOTA foundation models in the case of fine-tuning, regimes for Mantis on the 151-D benchmark. The best epoch accuracy is averaged over 3 random seeds and reported with the standard deviation.

	UniTS	GPT4TS	NuTime	MOMENT	Mantis		UniTS	GPT4TS	NuTime	MOMENT	Mantis
ACSF1	0.6933 \pm 0.0351	0.49 \pm 0.0265	0.6733 \pm 0.0321	0.6033 \pm 0.0379	0.7433 \pm 0.0115	InsectEPGSmallTrain	0.6667 \pm 0.0145	1.0 \pm 0.0	1.0 \pm 0.0	0.8969 \pm 0.0023	1.0 \pm 0.0
Adiac	0.5772 \pm 0.0074	0.3572 \pm 0.0059	0.7349 \pm 0.0141	0.5823 \pm 0.0296	0.776 \pm 0.003	InsectWingbeatSound	0.5726 \pm 0.0016	0.6165 \pm 0.0069	0.619 \pm 0.0048	0.6019 \pm 0.0034	0.5961 \pm 0.0051
AllGestureWimoteX	0.469 \pm 0.0224	0.4895 \pm 0.0105	0.6386 \pm 0.0038	0.7 \pm 0.0103	0.7169 \pm 0.005	ItalyPowerDemand	0.964 \pm 0.0019	0.9637 \pm 0.0011	0.9669 \pm 0.0002	0.9624 \pm 0.0006	0.9624 \pm 0.0015
AllGestureWimoteY	0.5338 \pm 0.0242	0.5062 \pm 0.0116	0.7152 \pm 0.0103	0.7081 \pm 0.0343	0.7948 \pm 0.0097	LargeKitchenAppliances	0.6942 \pm 0.0178	0.5156 \pm 0.0285	0.824 \pm 0.0116	0.8693 \pm 0.0232	0.8516 \pm 0.0111
AllGestureWimoteZ	0.4595 \pm 0.0159	0.4719 \pm 0.0119	0.6419 \pm 0.0058	0.6976 \pm 0.0218	0.73 \pm 0.01	Lightning2	0.7486 \pm 0.0063	0.7268 \pm 0.025	0.776 \pm 0.025	0.7978 \pm 0.025	0.8087 \pm 0.0189
ArrowHead	0.6895 \pm 0.0087	0.7638 \pm 0.0033	0.8305 \pm 0.0033	0.779 \pm 0.0082	0.821 \pm 0.0089	Lightning7	0.5571 \pm 0.0209	0.5982 \pm 0.0079	0.7032 \pm 0.0519	0.7717 \pm 0.0209	0.7397 \pm 0.0062
BME	0.8867 \pm 0.1048	0.9444 \pm 0.0102	1.0 \pm 0.0	0.98 \pm 0.0231	0.9956 \pm 0.0077	Mallat	0.8736 \pm 0.011	0.92 \pm 0.0258	0.9508 \pm 0.0191	0.9205 \pm 0.026	0.9404 \pm 0.0372
Beef	0.6667 \pm 0.0333	0.8 \pm 0.0577	0.8222 \pm 0.0192	0.8 \pm 0.0577	0.7 \pm 0.0333	Meal	0.9111 \pm 0.0255	0.6944 \pm 0.2269	0.9611 \pm 0.0255	0.6444 \pm 0.0674	0.9333 \pm 0.0289
BeetleFly	0.7167 \pm 0.0289	0.8167 \pm 0.0289	0.8833 \pm 0.0764	0.8 \pm 0.15	0.8833 \pm 0.0764	MedicalImages	0.6553 \pm 0.0026	0.611 \pm 0.0201	0.7513 \pm 0.0149	0.7206 \pm 0.029	0.7662 \pm 0.0178
BirdChicken	0.6167 \pm 0.1155	0.6167 \pm 0.0289	0.85 \pm 0.05	0.7667 \pm 0.0289	0.9 \pm 0.05	MelbournePedestrian	0.8711 \pm 0.0025	0.9351 \pm 0.0037	0.9601 \pm 0.0019	0.8795 \pm 0.0055	0.9552 \pm 0.001
CBF	0.8507 \pm 0.0192	0.8596 \pm 0.0083	0.9652 \pm 0.0046	0.9767 \pm 0.0172	0.9848 \pm 0.0074	MiddlePhalanxOutlineAgeGroup	0.6039 \pm 0.0065	0.6104 \pm 0.0065	0.5368 \pm 0.0198	0.6126 \pm 0.0327	0.5996 \pm 0.0209
Car	0.6278 \pm 0.0509	0.8 \pm 0.0167	0.8444 \pm 0.0096	0.8778 \pm 0.0419	0.8722 \pm 0.0096	MiddlePhalanxOutlineCorrect	0.827 \pm 0.0241	0.6518 \pm 0.0436	0.7938 \pm 0.0248	0.8076 \pm 0.0034	0.8339 \pm 0.0139
Chinatown	0.9776 \pm 0.0045	0.9718 \pm 0.0089	0.9738 \pm 0.0	0.9708 \pm 0.0127	0.9718 \pm 0.0017	MiddlePhalanxTW	0.5779 \pm 0.0234	0.5909 \pm 0.0	0.4632 \pm 0.015	0.5606 \pm 0.0037	0.4827 \pm 0.03
ChlorineConcentration	0.6424 \pm 0.0203	0.5733 \pm 0.0091	0.6718 \pm 0.008	0.6289 \pm 0.0178	0.6971 \pm 0.0112	MixedShapesSmallTrain	0.7281 \pm 0.0569	0.8115 \pm 0.0111	0.9281 \pm 0.0054	0.8357 \pm 0.0063	0.9531 \pm 0.0038
CinCECGTorso	0.585 \pm 0.0194	0.791 \pm 0.0353	0.9302 \pm 0.0067	0.743 \pm 0.008	0.781 \pm 0.0173	MusStrain	0.8339 \pm 0.0081	0.8243 \pm 0.0062	0.9609 \pm 0.0037	0.8347 \pm 0.0264	0.9068 \pm 0.0174
Coffee	1.0 \pm 0.0	1.0 \pm 0.0	1.0 \pm 0.0	0.9881 \pm 0.0206	1.0 \pm 0.0	NonInvasiveFetalECGThorax1	0.8879 \pm 0.0059	0.7774 \pm 0.0152	0.9342 \pm 0.0076	0.753 \pm 0.0237	0.9086 \pm 0.0063
Computers	0.6093 \pm 0.0046	0.62 \pm 0.0106	0.812 \pm 0.0174	0.6747 \pm 0.0295	0.7813 \pm 0.0162	NonInvasiveFetalECGThorax2	0.9137 \pm 0.0015	0.839 \pm 0.0098	0.9381 \pm 0.0046	0.7995 \pm 0.0033	0.9216 \pm 0.0055
CrickeT	0.5145 \pm 0.0074	0.5231 \pm 0.0143	0.7453 \pm 0.0039	0.7915 \pm 0.0192	0.796 \pm 0.009	OSULLeaf	0.5482 \pm 0.0391	0.4669 \pm 0.018	0.8967 \pm 0.0286	0.8017 \pm 0.0219	0.9642 \pm 0.0024
CrickeTY	0.541 \pm 0.0194	0.5419 \pm 0.0099	0.7479 \pm 0.0164	0.7487 \pm 0.0271	0.806 \pm 0.0141	OSULFoil	0.4778 \pm 0.0385	0.4889 \pm 0.0385	0.7778 \pm 0.0385	0.4667 \pm 0.0667	0.8889 \pm 0.0069
CrickeTZ	0.5521 \pm 0.0292	0.5496 \pm 0.0039	0.7701 \pm 0.0246	0.8068 \pm 0.0218	0.8043 \pm 0.0415	PhalangesOutlinesCorrect	0.8015 \pm 0.0037	0.6437 \pm 0.0041	0.8263 \pm 0.0031	0.803 \pm 0.0047	0.8162 \pm 0.0128
Crop	0.7184 \pm 0.0059	0.7311 \pm 0.0033	0.7574 \pm 0.0022	0.717 \pm 0.0071	0.7444 \pm 0.0039	Phoneme	0.1431 \pm 0.0086	0.1466 \pm 0.0023	0.2973 \pm 0.0081	0.2904 \pm 0.009	0.3214 \pm 0.0059
DationSizeReduction	0.9118 \pm 0.0259	0.9401 \pm 0.0061	0.9314 \pm 0.0425	0.9325 \pm 0.0576	0.9146 \pm 0.0136	PickupGestureWimoteZ	0.564 \pm 0.02	0.7133 \pm 0.0221	0.7267 \pm 0.0115	0.72 \pm 0.0	0.72 \pm 0.0
DistalPhalanxOutlineAgeGroup	0.7434 \pm 0.0083	0.7218 \pm 0.0042	0.7386 \pm 0.015	0.7362 \pm 0.0272	0.769 \pm 0.0259	Plane	0.9524 \pm 0.0165	0.9778 \pm 0.0055	1.0 \pm 0.0	0.9873 \pm 0.0115	1.0 \pm 0.0
DistalPhalanxOutlineCorrect	0.75 \pm 0.0166	0.6932 \pm 0.0084	0.7705 \pm 0.0302	0.7452 \pm 0.02	0.717 \pm 0.0158	PowerCons	0.954 \pm 0.02	1.0 \pm 0.0	0.9889 \pm 0.0111	0.9167 \pm 0.0111	0.9944 \pm 0.0096
DistalPhalanxTW	0.6691 \pm 0.0125	0.6978 \pm 0.0125	0.6978 \pm 0.0216	0.6451 \pm 0.03	0.6954 \pm 0.0231	ProximalPhalanxOutlineAgeGroup	0.8407 \pm 0.0157	0.8016 \pm 0.0203	0.8553 \pm 0.0102	0.8455 \pm 0.0123	0.8455 \pm 0.0246
DodgerLoopDay	0.45 \pm 0.0331	0.5542 \pm 0.0564	0.5458 \pm 0.0688	0.5292 \pm 0.0641	0.625 \pm 0.025	ProximalPhalanxOutlineCorrect	0.8568 \pm 0.0052	0.8179 \pm 0.0034	0.9072 \pm 0.006	0.8259 \pm 0.0221	0.8763 \pm 0.0209
DodgerLoopGame	0.8308 \pm 0.0233	0.8551 \pm 0.0192	0.8213 \pm 0.0649	0.8599 \pm 0.0233	0.884 \pm 0.0145	RefrigeratorTW	0.7951 \pm 0.0098	0.7967 \pm 0.0102	0.8179 \pm 0.0056	0.787 \pm 0.0102	0.7772 \pm 0.0314
DodgerLoopWeekend	0.9639 \pm 0.0072	0.9855 \pm 0.0	0.9783 \pm 0.0126	0.9783 \pm 0.0126	0.9783 \pm 0.0	RingPhalangesDevices	0.4658 \pm 0.0248	0.3956 \pm 0.0126	0.5511 \pm 0.0227	0.4999 \pm 0.0306	0.4916 \pm 0.0111
ECC200	0.8767 \pm 0.0611	0.8467 \pm 0.0551	0.87 \pm 0.01	0.8867 \pm 0.0231	0.8567 \pm 0.0058	Rock	0.6133 \pm 0.0945	0.5933 \pm 0.0503	0.68 \pm 0.02	0.6733 \pm 0.0611	0.7133 \pm 0.0231
ECC5000	0.9314 \pm 0.0042	0.9408 \pm 0.0019	0.9379 \pm 0.0001	0.9325 \pm 0.0001	0.9338 \pm 0.0081	ScreenType	0.3556 \pm 0.0041	0.3956 \pm 0.0126	0.5289 \pm 0.0434	0.4213 \pm 0.0116	0.4782 \pm 0.0041
ECGFiveDays	0.8459 \pm 0.054	0.8784 \pm 0.076	0.9621 \pm 0.0084	0.7944 \pm 0.0373	0.9146 \pm 0.0292	ShakeGestureWimoteZ	0.6067 \pm 0.0416	0.6867 \pm 0.0115	0.9133 \pm 0.0231	0.9067 \pm 0.0115	0.92 \pm 0.0
ElectricQuakes	0.738 \pm 0.033	0.7338 \pm 0.0072	0.7482 \pm 0.0	0.7578 \pm 0.0166	0.748 \pm 0.0	ShapeletSim	0.6981 \pm 0.0651	0.5074 \pm 0.0128	0.8852 \pm 0.0534	1.0 \pm 0.0	1.0 \pm 0.0
ElectricDevices	0.6194 \pm 0.0046	0.5776 \pm 0.0173	0.7112 \pm 0.0109	0.6666 \pm 0.0204	0.745 \pm 0.0049	ShapesAll	0.67 \pm 0.012	0.6833 \pm 0.0029	0.8856 \pm 0.0067	0.8039 \pm 0.0108	0.8906 \pm 0.0059
FaceAll	0.7335 \pm 0.0343	0.7247 \pm 0.0402	0.8385 \pm 0.0098	0.8012 \pm 0.008	0.8305 \pm 0.0031	SmallKitchenAppliances	0.6276 \pm 0.032	0.5529 \pm 0.0171	0.7822 \pm 0.0015	0.6756 \pm 0.0161	0.7929 \pm 0.0031
FaceFour	0.6515 \pm 0.0347	0.8295 \pm 0.0301	0.9318 \pm 0.0227	0.8371 \pm 0.0853	0.977 \pm 0.0114	SmoothSubspace	0.8156 \pm 0.0102	0.8911 \pm 0.0038	0.9889 \pm 0.0038	0.7733 \pm 0.0291	0.9978 \pm 0.0038
FacesUCR	0.7197 \pm 0.0078	0.7932 \pm 0.0047	0.8846 \pm 0.0127	0.835 \pm 0.0014	0.9148 \pm 0.0071	SonyAIBORobotSurface1	0.721 \pm 0.0846	0.6267 \pm 0.0105	0.8525 \pm 0.0189	0.7604 \pm 0.0204	0.8142 \pm 0.0133
FiftyWords	0.6223 \pm 0.0104	0.6615 \pm 0.0058	0.7875 \pm 0.0083	0.7861 \pm 0.0222	0.813 \pm 0.0083	SonyAIBORobotSurface2	0.829 \pm 0.0252	0.8454 \pm 0.0205	0.8506 \pm 0.0115	0.8765 \pm 0.0276	0.8996 \pm 0.0112
Fish	0.7943 \pm 0.0396	0.8133 \pm 0.0119	0.9524 \pm 0.0119	0.9162 \pm 0.0201	0.9716 \pm 0.0099	Strawberry	0.9577 \pm 0.0172	0.7261 \pm 0.0788	0.9712 \pm 0.0031	0.9459 \pm 0.0064	0.9667 \pm 0.0078
ForDA	0.9202 \pm 0.0049	0.7207 \pm 0.0798	0.9225 \pm 0.0095	0.9202 \pm 0.0271	0.9343 \pm 0.0046	SwedishLeaf	0.88 \pm 0.0085	0.8203 \pm 0.0305	0.9573 \pm 0.0024	0.9376 \pm 0.007	0.9712 \pm 0.0042
ForDB	0.7634 \pm 0.0043	0.6107 \pm 0.0567	0.7922 \pm 0.0126	0.8173 \pm 0.0125	0.7979 \pm 0.0135	Symbols	0.8211 \pm 0.0348	0.8003 \pm 0.0243	0.9779 \pm 0.0053	0.9481 \pm 0.0192	0.9889 \pm 0.0107
FreezerRegularTrain	0.911 \pm 0.0171	0.8884 \pm 0.0329	0.9942 \pm 0.0014	0.9876 \pm 0.0056	0.9927 \pm 0.0041	SyntheticControl	0.95 \pm 0.0088	0.9622 \pm 0.0117	0.9889 \pm 0.0051	0.9889 \pm 0.0019	0.9944 \pm 0.0038
FreezerSmallTrain	0.6713 \pm 0.012	0.6614 \pm 0.0094	0.9537 \pm 0.029	0.8206 \pm 0.0695	0.9667 \pm 0.0098	ToeSegmentation1	0.8012 \pm 0.0373	0.5687 \pm 0.0051	0.9459 \pm 0.0101	0.9384 \pm 0.0049	0.9664 \pm 0.0067
Fungi	0.6272 \pm 0.0306	0.7061 \pm 0.0124	0.7294 \pm 0.0135	0.69 \pm 0.035	0.7778 \pm 0.0031	ToeSegmentation2	0.7974 \pm 0.016	0.6923 \pm 0.0353	0.8974 \pm 0.0089	0.9308 \pm 0.0204	0.9231 \pm 0.0077
GestureMidAirD1	0.5256 \pm 0.0347	0.56									

Table 5: Mantis without and with the differential block used in the Token Generator Unit. The two models are compared under the feature extraction regime on the 159-D benchmark with results averaged over 3 random seeds.

	Mantis w/o Diff	Mantis w/ Diff		Mantis w/o Diff	Mantis w/ Diff
ACSF1	0.6433 ± 0.0252	0.6133 ± 0.0208	ItalyPowerDemand	0.8996 ± 0.003	0.9077 ± 0.0035
Adiac	0.6931 ± 0.0068	0.7332 ± 0.0039	LargeKitchenAppliances	0.7662 ± 0.0094	0.7804 ± 0.0041
AllGestureWiimoteX	0.641 ± 0.0054	0.6705 ± 0.0044	Lightning2	0.7268 ± 0.0189	0.8033 ± 0.0
AllGestureWiimoteY	0.6343 ± 0.0071	0.6671 ± 0.0057	Lightning7	0.6941 ± 0.0209	0.7763 ± 0.0285
AllGestureWiimoteZ	0.631 ± 0.0068	0.6695 ± 0.0033	Mallat	0.8904 ± 0.0074	0.8903 ± 0.0137
ArrowHead	0.7543 ± 0.0057	0.7105 ± 0.0175	Meat	0.95 ± 0.0167	0.9389 ± 0.0096
BME	0.8689 ± 0.0038	0.9311 ± 0.0038	MedicalImages	0.682 ± 0.0033	0.7079 ± 0.0035
Beef	0.6 ± 0.0	0.6556 ± 0.0509	MelbournePedestrian	0.9083 ± 0.0018	0.9016 ± 0.0031
BeetleFly	0.9 ± 0.05	0.85 ± 0.05	MiddlePhalanxOutlineAgeGroup	0.5952 ± 0.0163	0.5801 ± 0.0099
BirdChicken	0.8833 ± 0.0289	1.0 ± 0.0	MiddlePhalanxOutlineCorrect	0.8087 ± 0.004	0.8099 ± 0.0099
CBF	0.9937 ± 0.0017	0.993 ± 0.0013	MiddlePhalanxTW	0.5433 ± 0.0099	0.5368 ± 0.0099
Car	0.7389 ± 0.0096	0.7722 ± 0.0419	MixedShapesRegularTrain	0.8995 ± 0.0017	0.943 ± 0.0044
Chinatown	0.8678 ± 0.0131	0.8737 ± 0.0168	MixedShapesSmallTrain	0.8476 ± 0.0069	0.8961 ± 0.0004
ChlorineConcentration	0.6729 ± 0.0017	0.6806 ± 0.0019	MoteStrain	0.9255 ± 0.0005	0.9137 ± 0.0136
CinCECGTorso	0.6664 ± 0.0098	0.6611 ± 0.0036	NonInvasiveFetalECGThorax1	0.7837 ± 0.0058	0.6222 ± 0.0037
Coffee	0.9286 ± 0.0	0.9524 ± 0.0206	NonInvasiveFetalECGThorax2	0.8053 ± 0.0043	0.6872 ± 0.0025
Computers	0.7267 ± 0.0046	0.7373 ± 0.0092	OSULeaf	0.7617 ± 0.0048	0.8747 ± 0.0104
CricketX	0.706 ± 0.0146	0.7368 ± 0.0171	OliveOil	0.8889 ± 0.0192	0.9333 ± 0.0
CricketY	0.7496 ± 0.0107	0.7504 ± 0.0065	PLAID	0.8442 ± 0.0043	0.8181 ± 0.0047
CricketZ	0.7889 ± 0.003	0.7906 ± 0.0039	PhalangesOutlinesCorrect	0.7949 ± 0.0031	0.7786 ± 0.0042
Crop	0.6879 ± 0.0009	0.6756 ± 0.0018	Phoneme	0.289 ± 0.0024	0.323 ± 0.0034
DiatomSizeReduction	0.7963 ± 0.0136	0.8845 ± 0.0019	PickupGestureWiimoteZ	0.7 ± 0.02	0.74 ± 0.02
DistalPhalanxOutlineAgeGroup	0.7482 ± 0.0125	0.789 ± 0.015	PigAirwayPressure	0.4663 ± 0.0	0.484 ± 0.0147
DistalPhalanxOutlineCorrect	0.7681 ± 0.0036	0.75 ± 0.0126	PigArtPressure	0.9071 ± 0.0028	0.9103 ± 0.0028
DistalPhalanxTW	0.6571 ± 0.0042	0.6859 ± 0.011	PigCVP	0.8269 ± 0.0048	0.7837 ± 0.0127
DodgerLoopDay	0.5583 ± 0.0191	0.55 ± 0.0217	Plane	1.0 ± 0.0	1.0 ± 0.0
DodgerLoopGame	0.6618 ± 0.0274	0.7585 ± 0.0221	PowerCons	0.9315 ± 0.014	0.9093 ± 0.0032
DodgerLoopWeekend	0.9758 ± 0.0042	0.9517 ± 0.0084	ProximalPhalanxOutlineAgeGroup	0.8537 ± 0.0049	0.8537 ± 0.0049
ECG200	0.86 ± 0.02	0.82 ± 0.01	ProximalPhalanxOutlineCorrect	0.8213 ± 0.0034	0.8202 ± 0.0086
ECG5000	0.9283 ± 0.0011	0.9211 ± 0.001	ProximalPhalanxTW	0.7707 ± 0.0098	0.7691 ± 0.0028
ECGFiveDays	0.8668 ± 0.0159	0.909 ± 0.0218	RefrigerationDevices	0.5138 ± 0.0101	0.504 ± 0.0122
EOGHorizontalSignal	0.5875 ± 0.0188	0.5875 ± 0.0089	Rock	0.6933 ± 0.0088	0.7133 ± 0.0115
EOGVerticalSignal	0.4365 ± 0.0127	0.4751 ± 0.0	ScreenType	0.5031 ± 0.0101	0.4649 ± 0.0134
Earthquakes	0.753 ± 0.0042	0.7482 ± 0.0	SemgHandGenderCh2	0.8772 ± 0.0051	0.9189 ± 0.0086
ElectricDevices	0.7045 ± 0.0006	0.7226 ± 0.0026	SemgHandMovementCh2	0.7622 ± 0.0059	0.797 ± 0.0056
EthanolLevel	0.2873 ± 0.0117	0.2993 ± 0.011	SemgHandSubjectCh2	0.8304 ± 0.0114	0.8622 ± 0.0135
FaceAll	0.7992 ± 0.003	0.7815 ± 0.0074	ShakeGestureWiimoteZ	0.8733 ± 0.0115	0.8867 ± 0.0115
FaceFour	0.947 ± 0.0131	0.9508 ± 0.0066	ShapeletSim	0.963 ± 0.0032	0.9278 ± 0.0111
FacesUCR	0.8364 ± 0.0067	0.8354 ± 0.0054	ShapesAll	0.8189 ± 0.0107	0.8194 ± 0.0054
FiftyWords	0.5758 ± 0.0066	0.6462 ± 0.0096	SmallKitchenAppliances	0.8036 ± 0.0094	0.8089 ± 0.0081
Fish	0.9124 ± 0.0132	0.9333 ± 0.0066	SmoothSubspace	0.9289 ± 0.0102	0.9067 ± 0.0115
FordA	0.8328 ± 0.0012	0.8581 ± 0.0048	SonyAIBORobotSurface1	0.7682 ± 0.02	0.787 ± 0.0294
FordB	0.7198 ± 0.0096	0.7305 ± 0.0031	SonyAIBORobotSurface2	0.7964 ± 0.0184	0.8552 ± 0.0168
FreezerRegularTrain	0.9533 ± 0.0013	0.9374 ± 0.0043	StarLightCurves	0.9772 ± 0.0005	0.9759 ± 0.0005
FreezerSmallTrain	0.7556 ± 0.004	0.7942 ± 0.0059	Strawberry	0.9541 ± 0.0	0.9514 ± 0.0027
Fungi	0.81 ± 0.0062	0.8262 ± 0.0164	SwedishLeaf	0.9035 ± 0.0024	0.9275 ± 0.0009
GestureMidAirD1	0.6359 ± 0.0194	0.659 ± 0.0044	Symbols	0.9357 ± 0.0126	0.9698 ± 0.0056
GestureMidAirD2	0.6308 ± 0.0077	0.6154 ± 0.0077	SyntheticControl	0.9478 ± 0.0051	0.9767 ± 0.0067
GestureMidAirD3	0.341 ± 0.016	0.3282 ± 0.016	ToeSegmentation1	0.9415 ± 0.0154	0.9635 ± 0.0067
GesturePebbleZ1	0.9302 ± 0.0	0.9283 ± 0.0034	ToeSegmentation2	0.8718 ± 0.0364	0.9282 ± 0.0044
GesturePebbleZ2	0.9051 ± 0.011	0.9219 ± 0.0256	Trace	1.0 ± 0.0	1.0 ± 0.0
GunPoint	0.9711 ± 0.0038	0.98 ± 0.0067	TwoLeadECG	0.9839 ± 0.0056	0.9962 ± 0.0005
GunPointAgeSpan	0.9736 ± 0.0018	0.9905 ± 0.0	TwoPatterns	0.8987 ± 0.0034	0.8802 ± 0.0079
GunPointMaleVersusFemale	0.9937 ± 0.0	0.9958 ± 0.0018	UMD	0.9491 ± 0.008	0.9722 ± 0.0069
GunPointOldVersusYoung	0.9968 ± 0.0	0.9968 ± 0.0	UWaveGestureLibraryAll	0.8283 ± 0.0036	0.8458 ± 0.0057
Ham	0.6 ± 0.0095	0.673 ± 0.0145	UWaveGestureLibraryX	0.7487 ± 0.0012	0.7696 ± 0.0028
HandOutlines	0.9063 ± 0.0056	0.9162 ± 0.0072	UWaveGestureLibraryY	0.6676 ± 0.0017	0.6874 ± 0.0022
Haptics	0.4448 ± 0.0162	0.4968 ± 0.0032	UWaveGestureLibraryZ	0.7082 ± 0.0023	0.7324 ± 0.0036
Herring	0.6979 ± 0.018	0.6667 ± 0.0239	Wafer	0.9794 ± 0.0006	0.9903 ± 0.0003
HouseTwenty	0.944 ± 0.0049	0.9412 ± 0.0	Wine	0.6728 ± 0.0107	0.7901 ± 0.0107
InlineSkate	0.3703 ± 0.0107	0.363 ± 0.0136	WordSynonyms	0.4932 ± 0.0048	0.5502 ± 0.0081
InsectEPGRegularTrain	1.0 ± 0.0	1.0 ± 0.0	Worms	0.6017 ± 0.0075	0.6537 ± 0.027
InsectEPGSmallTrain	1.0 ± 0.0	1.0 ± 0.0	WormsTwoClass	0.6926 ± 0.0198	0.8139 ± 0.0198
InsectWingbeatSound	0.4739 ± 0.006	0.519 ± 0.0044	Yoga	0.8164 ± 0.001	0.815 ± 0.0012
Blink	0.9948 ± 0.0013	0.9993 ± 0.0013	Handwriting	0.3027 ± 0.01	0.339 ± 0.01
EMOPain	0.8423 ± 0.0056	0.8385 ± 0.0016	Heartbeat	0.7675 ± 0.0157	0.798 ± 0.017
MotionSenseHAR	0.9925 ± 0.0038	0.9975 ± 0.0022	InsectWingbeatSubset	0.5837 ± 0.0064	0.607 ± 0.007
SharePriceIncrease	0.6877 ± 0.0026	0.6836 ± 0.0049	JapaneseVowels	0.9514 ± 0.0047	0.963 ± 0.006
ArticulatoryWordRecognition	0.9911 ± 0.0019	0.993 ± 0.003	LSST	0.5884 ± 0.0015	0.605 ± 0.002
BasicMotions	1.0 ± 0.0	1.0 ± 0.0	Libras	0.8815 ± 0.017	0.898 ± 0.008
CharacterTrajectories	0.9352 ± 0.0025	0.94 ± 0.001	MotorImagery	0.5267 ± 0.0208	0.55 ± 0.036
Cricket	1.0 ± 0.0	1.0 ± 0.0	NATOPS	0.9 ± 0.0056	0.907 ± 0.013
DuckDuckGeese	0.38 ± 0.0529	0.407 ± 0.031	PEMS-SF	0.9807 ± 0.0067	0.985 ± 0.013
ERing	0.8284 ± 0.0311	0.941 ± 0.01	PhonemeSpectra	0.2587 ± 0.0012	0.273 ± 0.008
EigenWorms	0.7557 ± 0.0076	0.753 ± 0.016	RacketSports	0.9123 ± 0.0137	0.923 ± 0.004
Epilepsy	0.9928 ± 0.0072	0.995 ± 0.004	SelfRegulationSCP1	0.7611 ± 0.0034	0.804 ± 0.011
EthanolConcentration	0.3308 ± 0.0076	0.27 ± 0.01	SelfRegulationSCP2	0.4796 ± 0.0064	0.476 ± 0.045
FaceDetection	0.5138 ± 0.0078	0.526 ± 0.002	SpokenArabicDigits	0.8172 ± 0.0081	0.839 ± 0.005
FingerMovements	0.5333 ± 0.0058	0.54 ± 0.035	UWaveGestureLibrary	0.8188 ± 0.0083	0.814 ± 0.01
HandMovementDirection	0.3108 ± 0.0135	0.212 ± 0.041	Best Count	59	109

Table 6: Comparison of different fine-tuning regimes for Mantis on the 151-D benchmark. The last epoch accuracy is averaged over 3 random seeds and reported with the standard deviation.

	RF	Head	Scratch	Full		RF	Head	Scratch	Full
ACSF1	0.6133±0.0208	0.6±0.0	0.57±0.0693	0.7033 ±0.0551	ItalyPowerDemand	0.9077±0.0035	0.9051±0.0048	0.9644 ±0.0034	0.953±0.0006
Adiac	0.7332±0.0039	0.5857±0.0051	0.7315±0.0	0.8133 ±0.0	LargeKitchenAppliances	0.7804±0.0041	0.784±0.008	0.8676 ±0.0147	0.8542±0.0094
AllGestureWiimoteX	0.6705±0.0044	0.5471±0.0014	0.6838±0.0073	0.7924 ±0.0073	Lightning2	0.8033±0.0	0.8251±0.0189	0.8525 ±0.0328	0.8197±0.0
AllGestureWiimoteY	0.6671±0.0057	0.5595±0.0044	0.7224±0.0084	0.8033 ±0.0084	Lightning7	0.7763±0.0285	0.7671±0.0137	0.6986 ±0.0137	0.8219 ±0.0137
AllGestureWiimoteZ	0.6695±0.0033	0.5414±0.0014	0.6271±0.0289	0.7443 ±0.0076	Mallat	0.8903±0.0137	0.7765±0.0019	0.8691±0.0111	0.9389 ±0.0146
ArrowHead	0.7105±0.0175	0.7276±0.0119	0.7752±0.0282	0.8114 ±0.0206	Meat	0.9389±0.0096	0.8889±0.0255	0.8167±0.0928	0.9444 ±0.0385
BME	0.9311±0.0038	0.8756±0.0139	0.9844±0.0038	1.0 ±0.0	MedicalImages	0.7079±0.0035	0.6939±0.0142	0.7412±0.0102	0.8013 ±0.0154
BeetleFly	0.6556±0.0509	0.6111±0.0192	0.7667±0.0882	0.7889 ±0.0192	MelbournePedestrian	0.9016±0.0031	0.8922±0.0038	0.9576±0.0037	0.9703 ±0.0005
BirdChicken	1.0 ±0.0	1.0 ±0.0	0.8333±0.0289	1.0 ±0.0	MiddlePhalanxOutlineAgeGroup	0.5801±0.0099	0.5823 ±0.0228	0.5043±0.0293	0.5325±0.0208
CBF	0.993±0.0013	0.9941±0.0006	0.9844±0.0185	0.9993 ±0.0013	MiddlePhalanxOutlineCorrect	0.8099±0.0099	0.8007±0.0124	0.7927±0.0086	0.8522 ±0.0091
Car	0.7722±0.0419	0.7778±0.0192	0.7056±0.0192	0.8833 ±0.0167	MiddlePhalanxTW	0.5368 ±0.0099	0.5087±0.0163	0.5152±0.0262	0.5087±0.0187
Chinatown	0.8737±0.0168	0.8785±0.0094	0.9582±0.0067	0.9767 ±0.0077	MixedShapesRegularTrain	0.943±0.0044	0.9387±0.0037	0.9555±0.0043	0.9801 ±0.0006
ChlorineConcentration	0.6806±0.0019	0.5688±0.0011	0.7494±0.0034	0.7718 ±0.01	MixedShapesSmallTrain	0.8961±0.0004	0.8936±0.0054	0.8843±0.0116	0.9567 ±0.0041
CinCECGTorso	0.6611±0.0036	0.7176±0.0044	0.7802±0.019	0.8539 ±0.0096	MoteStrain	0.9137±0.0136	0.8988±0.0112	0.9087±0.0095	0.9241 ±0.0042
Coffee	0.9524±0.0206	0.9643±0.0	0.9881±0.0206	1.0 ±0.0	NonInvasiveFetalECGThorax1	0.6222±0.0037	0.6712±0.0018	0.9035±0.0016	0.936 ±0.0056
Computers	0.7373±0.0092	0.7093±0.0129	0.7053±0.022	0.7467 ±0.0205	NonInvasiveFetalECGThorax2	0.6872±0.0025	0.712±0.004	0.9152±0.0013	0.9445 ±0.0018
CricketX	0.7368±0.0171	0.6966±0.003	0.7538±0.0268	0.8205 ±0.0136	OSULeaf	0.8747±0.0104	0.8719±0.0109	0.8609±0.0104	0.9573 ±0.0086
CricketY	0.7504±0.0065	0.7043±0.003	0.7812±0.003	0.8214 ±0.0039	OliveOil	0.9333 ±0.0	0.4±0.0	0.6889±0.0192	0.9222±0.0509
CricketZ	0.7906±0.0039	0.7333±0.0077	0.7829±0.0082	0.8462 ±0.0039	PLAID	0.8181±0.0047	0.545±0.0047	0.897±0.0084	0.9199 ±0.0032
Crop	0.6756±0.0018	0.6738±0.0004	0.7558±0.0068	0.7631 ±0.0008	PhalangesOutlinesCorrect	0.7786±0.0042	0.7599±0.0051	0.8139±0.0029	0.8256 ±0.0125
DiatomSizeReduction	0.8845±0.0019	0.8889±0.017	0.8878±0.0075	0.9314 ±0.0033	Phoneme	0.323±0.0034	0.3224±0.0008	0.2683±0.0085	0.3434 ±0.0069
DistalPhalanxOutlineAgeGroup	0.789±0.015	0.8106 ±0.0042	0.6451±0.0324	0.7314±0.0111	PickupGestureWiimoteZ	0.74±0.02	0.7733±0.0611	0.6667±0.0231	0.7933 ±0.0306
DistalPhalanxOutlineCorrect	0.75±0.0126	0.7621±0.0042	0.7645±0.0072	0.7415±0.0091	PigAirwayPressure	0.484±0.0147	0.4455±0.0169	0.1843±0.0182	0.5176 ±0.0194
DistalPhalanxTW	0.6859 ±0.011	0.6595±0.0083	0.6619±0.0125	0.6619±0.0072	PigArtPressure	0.9103 ±0.0028	0.8221±0.0173	0.6571±0.0028	0.9087±0.0127
DodgerLoopDay	0.55±0.0217	0.5292±0.026	0.55±0.0375	0.6125 ±0.025	PigCVP	0.7837±0.0127	0.7724±0.0073	0.4631±0.01	0.8894 ±0.0254
DodgerLoopGame	0.7585±0.0221	0.7126±0.0084	0.7633±0.0167	0.9324 ±0.0254	Plane	1.0 ±0.0	1.0 ±0.0	1.0 ±0.0	1.0 ±0.0
DodgerLoopWeekend	0.9517±0.0084	0.9758±0.0111	0.9831 ±0.0042	0.9831 ±0.0042	PowerCons	0.9093±0.0032	0.8852±0.0274	0.9926±0.0032	0.9889±0.0
ECG200	0.82±0.01	0.8033±0.0252	0.8167±0.0115	0.9067 ±0.0153	ProximalPhalanxOutlineAgeGroup	0.8537±0.0049	0.8732 ±0.0	0.8276±0.0241	0.8244±0.0049
ECG5000	0.9211±0.001	0.9185±0.0039	0.9301±0.0039	0.9402 ±0.0006	ProximalPhalanxOutlineCorrect	0.8202±0.0086	0.8477±0.0105	0.8923 ±0.0189	0.8889±0.0113
ECGFiveDays	0.909±0.0218	0.8668±0.0401	0.7093±0.0697	0.9512 ±0.0247	ProximalPhalanxTW	0.7691±0.0028	0.7675±0.0123	0.7789 ±0.0171	0.761±0.0176
EOGHorizontalSignal	0.5875±0.0089	0.5691±0.0083	0.6308±0.0142	0.6722 ±0.0097	RefrigerationDevices	0.504 ±0.0122	0.4978±0.0015	0.4907±0.008	0.4889±0.0056
EOGVerticalSignal	0.4751±0.0	0.4797±0.0131	0.5037±0.0162	0.5617 ±0.0148	Rock	0.7133±0.0115	0.7667±0.0231	0.7867±0.0306	0.8533 ±0.0115
Earthquakes	0.7482±0.0	0.7506 ±0.0042	0.7482±0.0216	0.7266±0.0114	ScreenType	0.4649±0.0134	0.4507±0.0092	0.4711±0.0126	0.5085 ±0.0189
ElectricDevices	0.7226±0.0026	0.7039±0.0008	0.7112±0.0091	0.7505 ±0.0068	SemgHandGenderCh2	0.9189±0.0086	0.8561±0.0019	0.9417±0.0133	0.9461 ±0.0212
EthanolLevel	0.2933±0.011	0.3173±0.0117	0.6087±0.0463	0.6773 ±0.1125	SemgHandMovementCh2	0.797±0.0056	0.5622±0.0174	0.8267±0.0212	0.8556 ±0.025
FaceAll	0.9508±0.0074	0.8053±0.0062	0.9469 ±0.0042	0.8544 ±0.0345	SemgHandSubjectCh2	0.8622±0.0135	0.7763±0.0064	0.9193±0.0168	0.9415 ±0.021
FaceFour	0.9508±0.0066	0.947±0.0131	0.7879±0.0237	0.9697 ±0.0151	ShakeGestureWiimoteZ	0.8867±0.0115	0.8933±0.0231	0.84±0.02	0.9333 ±0.0115
FacesUCR	0.8354±0.0054	0.8434±0.0101	0.88±0.0042	0.9411 ±0.0035	ShapeletSim	0.9278±0.0111	0.913±0.0064	0.9815±0.017	1.0 ±0.0
FiftyWords	0.6462±0.0096	0.7026±0.0178	0.8088±0.0	0.8571 ±0.0022	ShapesAll	0.8194±0.0054	0.8489±0.0051	0.8739±0.01	0.9039 ±0.0035
Fish	0.9333±0.0066	0.9333±0.0033	0.9143±0.0151	0.9714 ±0.0057	SmallKitchenAppliances	0.8089±0.0081	0.8293 ±0.0	0.7902±0.0081	0.7893±0.0071
FordA	0.8581±0.0048	0.8869±0.0016	0.9235±0.0015	0.9417 ±0.002	SmoothSubspace	0.9067±0.0115	0.9378±0.0168	0.98±0.0	0.9933 ±0.0
FordB	0.7305±0.0031	0.765±0.0026	0.7807±0.0096	0.8329 ±0.0068	SonyAIBORobotSurface1	0.787±0.0294	0.8236±0.0292	0.8264 ±0.0217	0.8103±0.0202
FreezerRegularTrain	0.9374±0.0043	0.8767±0.0088	0.9927±0.0026	0.9964 ±0.0015	SonyAIBORobotSurface2	0.8552±0.0168	0.8821±0.0063	0.8356±0.0221	0.9307 ±0.0028
FreezerSmallTrain	0.7942±0.0059	0.8085±0.0041	0.8469±0.0886	0.9602 ±0.0224	StarLightCurves	0.9759±0.0005	0.9785 ±0.0007	0.972±0.002	0.9768 ±0.0011
Fungi	0.8262±0.0164	0.8477±0.0224	0.9301±0.0108	0.9839 ±0.0142	Strawberry	0.9514±0.0027	0.9108±0.0047	0.9712 ±0.0095	0.9667±0.0041
GestureMidAirD1	0.659±0.0044	0.6026±0.0044	0.6872±0.016	0.7744 ±0.0044	SwedishLeaf	0.9275±0.0009	0.9253±0.0024	0.9419±0.0033	0.9701 ±0.0072
GestureMidAirD2	0.6154±0.0077	0.5256±0.016	0.6487±0.0118	0.6949 ±0.0194	Symbols	0.9698±0.0056	0.9668±0.0036	0.9199±0.018	0.9873 ±0.0061
GestureMidAirD3	0.3282±0.016	0.3128±0.0291	0.3897±0.032	0.459 ±0.0235	SyntheticControl	0.9767±0.0067	0.9844±0.0051	0.9667±0.0017	0.9944 ±0.0038
GesturePebbleZ1	0.9283±0.0034	0.9186±0.0116	0.907±0.0101	0.9341 ±0.0089	ToeSegmentation1	0.9635±0.0067	0.9532±0.0127	0.8684±0.0219	0.9737 ±0.0044
GesturePebbleZ2	0.9219±0.0256	0.9451 ±0.0097	0.8586±0.0256	0.8481±0.0167	ToeSegmentation2	0.9282±0.0044	0.9564 ±0.0089	0.8692±0.0231	0.9256±0.0044
GunPoint	0.98±0.0067	0.9822±0.0038	0.9733±0.0176	0.9978 ±0.0038	Trace	1.0 ±0.0	1.0 ±0.0	1.0 ±0.0	1.0 ±0.0
GunPointAgeSpan	0.9905±0.0	0.9821±0.0037	0.9905±0.0032	0.9968 ±0.0	TwoLeadECG	0.9962±0.0005	0.998 ±0.0005	0.9236±0.0279	0.9974±0.0015
GunPointMaleVersusFemale	0.9958±0.0018	0.9863±0.0048	0.9926±0.0018	0.9979 ±0.0037	TwoPatterns	0.8802±0.0079	0.892±0.0021	0.9997±0.0004	1.0 ±0.0
GunPointOldVersusYoung	0.9968 ±0.0	0.9968 ±0.0	0.9926±0.0018	0.9968 ±0.0	UMD	0.9722±0.0069	0.9792±0.0	0.9769±0.016	0.9931 ±0.0
Han	0.673±0.0145	0.6857±0.0252	0.727±0.0145	0.6762±0.0252	UWaveGestureLibraryAll	0.8458±0.0057	0.8733±0.0014	0.9718±0.0005	0.9746 ±0.001
HandOutlines	0.9162±0.0072	0.8928±0.0068	0.9279±0.0095	0.9459 ±0.0027	UWaveGestureLibraryX	0.7696±0.0028	0.7911±0.0017	0.8368±0.0058	0.8714 ±0.0021
Haptics	0.4968±0.0032	0.4665±0.0114	0.4708±0.0086	0.5487 ±0.0225	UWaveGestureLibraryY	0.6874±0.0022	0.7061±0.0024	0.7742±0.0027	0.807 ±0.0011
Herring	0.6667±0.0239	0.7031 ±0.0156	0.5365±0.0502	0.6042±0.0325	UWaveGestureLibraryZ	0.7324±0.0036	0.7581±0.002	0.7841±0.0011	0.8248 ±0.0011
HouseTwenty	0.9412±0.0	0.9496±0.0084	0.9132±0.0049	0.9748 ±0.0084	Wafer	0.9903±0.0003	0.9839±0.0069	0.9948±0.0008	0.9988 ±0.0005
InlineSkate	0.363±0.0136	0.3164±0.0119	0.383±0.0282	0.4388 ±0.0128	Wine	0.7901±0.0107	0.5926±0.0321	0.6296±0.0185	0.6914±0.0385
InsectEPGRegularTrain	1.0 ±0.0	1.0 ±0.0	0.9893±0.0046	1.0 ±0.0	WordSynonyms	0.5502±0.0081	0.4901±0.0128	0.6886±0.0059	0.7571 ±0.0054
InsectEPGSmallTrain	1.0 ±0.0	1.0 ±0.0	0.9424±0.0221	1.0 ±0.0	Worms	0.6537±0.027	0.7186±0.015	0.7143±0.026	0.7489 ±0.0075
InsectWingbeatSound	0.519±0.0044	0.4785±0.0092	0.5966±0.0146	0.6093 ±0.0148	WormsTwoClass	0.8139 ±0.0198	0.8139 ±0.0198	0.7879±0.0327	0.7965±0.0115
Blink	1.0 ±0.0	0.9963±0.0046	0.983±0.0051	1.0 ±0.0	Yoga	0.815±0.0012	0.7452±0.0013	0.8217±0.0099	0.9063 ±0.0021
MotionSenseHAR	1.0 ±0.0	0.9962±0.0	0.9874±0.0022	1.0 ±0.0	Handwriting	0.3392±0.01	0.4271±0.0113	0.3294±0.0116	0.4773 ±0.0119
SharePriceIncrease	0.6874 ±0.0	0.6718±0.001	0.617±0.0112	0.6342±0.0119	JapaneseVowels	0.9631±0.0056	0.9649±0.0	0.9315±0.0145	0.9757 ±0.0027
ArticularyWordRecognition	0.9933±0.0033	0.9933±0.0	0.9967 ±0.0	0.9933 ±0.0	LSST	0.6054±0.0021	0.6459±0.0006	0.666±0.0111	0.6741 ±0.0021
BasicMotions	1.0 ±0.0	1.0 ±0.0	1.0 ±0.0	1.0 ±0.0	Libras	0.8981±0.0085	0.8963±0.014	0.9185±0.0064	0.9278 ±0.0111
CharacterTrajectories	0.9396±0.0008	0.9673±0.0021	0.9789±0.0028	0.9912 ±0.0011	NATOPS	0.9074±0.0128	0.9259 ±0.0116	0.8079±0.0189	0.9255 ±0.0085
Cricket	1.0 ±0.0	0.9861±0.0	0.9861±0.0	1.0 ±0.0	PhonemeSpectra	0.2735±0.0078	0.2934±0.0022	0.2082±0.0067	0.3106 ±0.0081
ERing	0.9407±0.0098	0.9296±0							

Table 7: Comparison of different fine-tuning regimes for Mantis on the 151-D benchmark. The best epoch accuracy is averaged over 3 random seeds and reported with the standard deviation.

	RF	Head	Scratch	Full		RF	Head	Scratch	Full
ACSF1	0.6133±0.0208	0.62±0.0265	0.6433±0.0451	0.7467 ±0.0416	ItalyPowerDemand	0.9077±0.0035	0.9054±0.0046	0.9725 ±0.002	0.9572±0.0
Adiac	0.7332±0.0039	0.5857±0.0051	0.7613±0.0129	0.8295 ±0.0082	LargeKitchenAppliances	0.7804±0.0041	0.7876±0.0108	0.8853 ±0.0053	0.8676±0.0094
AllGestureWiimoteX	0.6705±0.0044	0.551±0.0008	0.6962±0.0058	0.8029 ±0.0065	Lightning2	0.8033±0.0	0.8251±0.0189	0.8798 ±0.025	0.8361±0.0
AllGestureWiimoteY	0.6671±0.0057	0.5614±0.0052	0.739±0.0008	0.8129 ±0.0089	Lightning7	0.7763±0.0285	0.7763±0.0209	0.7671±0.0137	0.8356 ±0.0137
AllGestureWiimoteZ	0.6695±0.0033	0.5467±0.0008	0.6367±0.0246	0.7481 ±0.0095	Mallat	0.8903±0.0137	0.7765±0.0019	0.9529±0.0077	0.9774 ±0.0122
ArrowHead	0.7105±0.0175	0.7276±0.0119	0.8±0.0286	0.8229 ±0.0297	Meat	0.9389±0.0096	0.8944±0.0255	0.9222±0.0509	0.9778 ±0.0096
BME	0.9311±0.0038	0.8756±0.0139	0.9933±0.0	1.0 ±0.0	MedicalImages	0.7079±0.0035	0.6961±0.0139	0.7605±0.0164	0.8127 ±0.0106
Beef	0.6556±0.0509	0.6222±0.0385	0.8222±0.0694	0.8667 ±0.0	MelbournePedestrian	0.9016±0.0031	0.8922±0.0033	0.9615±0.0038	0.9728 ±0.0014
BeetleFly	0.85±0.05	0.9 ±0.0	0.7±0.0	0.9 ±0.05	MiddlePhalanxOutlineAgeGroup	0.5801±0.0099	0.6126±0.0262	0.6407 ±0.0037	0.6385±0.0037
BirdChicken	1.0 ±0.0	1.0 ±0.0	0.9±0.0	1.0 ±0.0	MiddlePhalanxOutlineCorrect	0.8099±0.0099	0.8076±0.0119	0.8328±0.0159	0.8786 ±0.0079
CBF	0.993±0.0013	0.9941±0.0006	0.9922±0.008	0.9996 ±0.0006	MiddlePhalanxTW	0.5368±0.0099	0.5823±0.0228	0.5974 ±0.013	0.5931±0.0228
Car	0.7722±0.0419	0.7778±0.0192	0.8±0.0	0.9 ±0.0289	MixedShapesRegularTrain	0.943±0.0044	0.9388±0.0044	0.9625±0.0014	0.981 ±0.0005
Chinatown	0.8737±0.0168	0.8785±0.0094	0.964±0.0017	0.9776 ±0.0067	MixedShapesSmallTrain	0.8961±0.0004	0.8937±0.0054	0.8983±0.0114	0.9581 ±0.0046
ChlorineConcentration	0.6806±0.0019	0.5704±0.0011	0.753±0.0056	0.7788 ±0.0072	MoteStrain	0.9137±0.0136	0.9023±0.0113	0.9358±0.0009	0.9289±0.0085
CinCECGTorso	0.6611±0.0036	0.7179±0.0048	0.7901±0.0198	0.856 ±0.0077	NonInvasiveFetalECGThorax1	0.6222±0.0037	0.6733±0.0013	0.9113 ±0.0011	0.9411±0.0026
Coffee	0.9524±0.0206	0.9643±0.0	1.0 ±0.0	1.0 ±0.0	NonInvasiveFetalECGThorax2	0.6872±0.0025	0.715±0.0028	0.9176±0.0011	0.9481 ±0.0027
Computers	0.7373±0.0092	0.728±0.0069	0.7533±0.0162	0.7773 ±0.0046	OSULeaf	0.8747±0.0104	0.8719±0.0109	0.8774±0.0063	0.9647 ±0.0167
CricketX	0.7368±0.0171	0.6966±0.003	0.7812±0.0446	0.8282 ±0.0133	OliveOil	0.9333±0.0	0.4±0.0	0.8333±0.0	0.9556 ±0.0192
CricketY	0.7504±0.0065	0.7051±0.0026	0.8±0.0026	0.8385 ±0.0051	PLAID	0.8181±0.0047	0.5469±0.0022	0.9044±0.0047	0.9243 ±0.0039
CricketZ	0.7906±0.0039	0.7333±0.0077	0.7991±0.0097	0.8521 ±0.0082	PhalangesOutlinesCorrect	0.7786±0.0042	0.7692±0.0012	0.8322±0.0042	0.8539 ±0.0013
Crop	0.6756±0.0018	0.6745±0.0001	0.7566±0.0063	0.7702 ±0.0005	Phoneme	0.323±0.0034	0.3231±0.002	0.2795±0.0024	0.3499 ±0.0075
DiatomSizeReduction	0.8845±0.0019	0.8911±0.0191	0.9031±0.0147	0.9346 ±0.0043	PickupGestureWiimoteZ	0.74±0.02	0.7867±0.0702	0.7067±0.0306	0.8267 ±0.0306
DistalPhalanxOutlineAgeGroup	0.789±0.015	0.8106 ±0.0042	0.7506±0.011	0.7938±0.0032	PigAirwayPressure	0.484±0.0147	0.4519±0.0096	0.2035±0.0147	0.524 ±0.0173
DistalPhalanxOutlineCorrect	0.75±0.0126	0.7729±0.0055	0.8056 ±0.0091	0.7935±0.0036	PigArtPressure	0.9103±0.0028	0.8221±0.0173	0.6875±0.0	0.9135 ±0.0096
DistalPhalanxTW	0.6859±0.011	0.6763±0.0125	0.7266±0.0125	0.7338 ±0.019	PigCVP	0.7837±0.0127	0.7788±0.0	0.4984±0.01	0.8974 ±0.0222
DodgerLoopDay	0.55±0.0217	0.5292±0.026	0.6208±0.0191	0.6375 ±0.0125	Plane	1.0 ±0.0	1.0 ±0.0	1.0 ±0.0	1.0 ±0.0
DodgerLoopGame	0.7585±0.0221	0.7222±0.0111	0.843±0.0084	0.9541 ±0.0042	PowerCons	0.9093±0.0032	0.8944±0.02	0.9944 ±0.0	0.9889±0.0
DodgerLoopWeekend	0.9517±0.0084	0.9783±0.0126	0.9855 ±0.0	0.9855 ±0.0	ProximalPhalanxOutlineAgeGroup	0.8537±0.0049	0.8732±0.0	0.8113±0.0028	0.8829 ±0.0084
ECG200	0.82±0.01	0.8033±0.0252	0.8467±0.0115	0.9133 ±0.0115	ProximalPhalanxOutlineCorrect	0.8202±0.0086	0.8499±0.0086	0.9118±0.0086	0.9244 ±0.0034
ECG5000	0.9211±0.001	0.9185±0.0038	0.9411±0.0008	0.9459 ±0.0014	ProximalPhalanxTW	0.7691±0.0028	0.7789±0.0056	0.8179±0.0028	0.8211 ±0.0056
ECGFiveDays	0.909±0.0218	0.8668±0.0401	0.7855±0.0169	0.9694 ±0.014	RefrigerationDevices	0.504±0.0122	0.5298±0.0041	0.5538 ±0.0161	0.5431±0.0041
EOGHorizontalSignal	0.5875±0.0089	0.5783±0.0064	0.6703±0.0194	0.6934 ±0.012	Rock	0.7133±0.0115	0.7667±0.0231	0.82±0.02	0.8667 ±0.0115
EOGVerticalSignal	0.4751±0.0	0.4825±0.0105	0.5396±0.0058	0.5773 ±0.0073	ScreenType	0.4649±0.0134	0.4809±0.012	0.5182±0.0031	0.5511 ±0.0362
Earthquakes	0.7482±0.0	0.7506±0.0042	0.7866 ±0.015	0.7602±0.015	SemgHandGenderCh2	0.9189±0.0086	0.86±0.0033	0.9494±0.0098	0.9617 ±0.0145
ElectricDevices	0.7226±0.0026	0.7064±0.001	0.7448±0.0044	0.7643 ±0.005	SemgHandMovementCh2	0.797±0.0056	0.563±0.0168	0.8378±0.0204	0.8674 ±0.0278
EthanolLevel	0.2993±0.011	0.324±0.006	0.6987±0.0194	0.7393 ±0.1052	SemgHandSubjectCh2	0.8622±0.0135	0.7763±0.0064	0.9356±0.0102	0.9496 ±0.0181
FaceAll	0.7815±0.0074	0.8053±0.0062	0.9542 ±0.0036	0.8554±0.0343	ShapeGestureWiimoteZ	0.8867±0.0115	0.8933±0.0231	0.9±0.0	0.9667 ±0.0115
FaceFour	0.9508±0.0066	0.9508±0.0174	0.8485±0.0347	0.9811 ±0.0066	ShapeletSim	0.9278±0.0111	0.9167±0.0111	0.9815±0.017	1.0 ±0.0
FacesUCR	0.8354±0.0054	0.8437±0.0104	0.8816±0.0054	0.942 ±0.0061	ShapesAll	0.8194±0.0054	0.8517±0.0076	0.8817±0.0083	0.9078 ±0.001
FiftyWords	0.6462±0.0096	0.7026±0.0178	0.8176±0.0038	0.863 ±0.0013	SmallKitchenAppliances	0.8089±0.0081	0.8302±0.0115	0.8347±0.0053	0.8471 ±0.0108
Fish	0.9333±0.0066	0.9333±0.0033	0.939±0.0087	0.979 ±0.0087	SmoothSubspace	0.9067±0.0115	0.9378±0.0168	0.9844±0.0038	0.9978 ±0.0038
FordA	0.8581±0.0048	0.8881±0.0004	0.9301±0.0031	0.9477 ±0.0013	SonyAIBORobotSurface1	0.787±0.0294	0.8247±0.03	0.9257 ±0.0069	0.8763±0.0003
FordB	0.7305±0.0031	0.7704±0.0033	0.8115±0.0036	0.8477 ±0.0014	SonyAIBORobotSurface2	0.8552±0.0168	0.8821±0.0063	0.8583±0.0371	0.9339 ±0.001
FreezerRegularTrain	0.9374±0.0043	0.8767±0.0088	0.9971 ±0.0004	0.9967±0.0044	StarLightCurves	0.9759±0.0005	0.9788±0.0005	0.9757±0.0015	0.981 ±0.0006
FreezerSmallTrain	0.7942±0.0059	0.8092±0.0041	0.8601±0.073	0.9648 ±0.0219	Strawberry	0.9514±0.0027	0.9153±0.0041	0.9802 ±0.0031	0.9775±0.0016
Fungi	0.8262±0.0164	0.8477±0.0224	0.948±0.0164	0.9892 ±0.0108	SwedishLeaf	0.9275±0.0009	0.9253±0.0024	0.9456±0.0016	0.9744 ±0.0028
GestureMidAirD1	0.659±0.0044	0.6026±0.0044	0.7103±0.0089	0.7949 ±0.0044	Symbols	0.9698±0.0056	0.9668±0.0036	0.9263±0.0177	0.9893 ±0.0057
GestureMidAirD2	0.6154±0.0077	0.5282±0.0118	0.6974±0.0222	0.7205 ±0.0247	SyntheticControl	0.9767±0.0067	0.9844±0.0051	0.9811±0.0051	0.9956 ±0.0019
GestureMidAirD3	0.3282±0.016	0.3154±0.0266	0.4359±0.016	0.4795 ±0.0178	ToeSegmentation1	0.9635±0.0067	0.9591±0.011	0.8918±0.0198	0.9825 ±0.0044
GesturePebbleZ1	0.9283±0.0034	0.9186±0.0116	0.9322±0.0089	0.9574 ±0.0146	ToeSegmentation2	0.9282±0.0044	0.9564 ±0.0089	0.9205±0.0118	0.9462±0.0077
GesturePebbleZ2	0.9219±0.0256	0.9515 ±0.0097	0.8882±0.0193	0.9451±0.0159	Trace	1.0 ±0.0	1.0 ±0.0	1.0 ±0.0	1.0 ±0.0
GunPoint	0.98±0.0067	0.9822±0.0038	0.9867±0.0133	0.9978 ±0.0038	TwoLeadECG	0.9962±0.0005	0.9985 ±0.0005	0.9631±0.0066	0.9985 ±0.001
GunPointAgeSpan	0.9905±0.0	0.9821±0.0037	0.9947±0.0048	0.9989 ±0.0018	TwoPatterns	0.8802±0.0079	0.892±0.0021	0.9998±0.0004	1.0 ±0.0
GunPointMaleVersusFemale	0.9958±0.0018	0.9863±0.0048	0.9947±0.0018	1.0 ±0.0	UMD	0.9722±0.0069	0.9792±0.0	0.9884±0.008	0.9931 ±0.0
GunPointOldVersusYoung	0.9968±0.0	0.9968±0.0	0.9968±0.0	1.0 ±0.0	UWaveGestureLibraryAll	0.8458±0.0057	0.8739±0.0014	0.9737±0.0008	0.9752 ±0.0007
Ham	0.673±0.0145	0.7143±0.0252	0.8159 ±0.0198	0.7016±0.0198	UWaveGestureLibraryX	0.7696±0.0028	0.7916±0.002	0.843±0.0031	0.8728 ±0.0017
HandOutlines	0.9162±0.0072	0.8928±0.0068	0.945±0.0056	0.955 ±0.0016	UWaveGestureLibraryY	0.6874±0.0022	0.7065±0.0024	0.7772±0.0029	0.8117 ±0.0003
Haptics	0.4968±0.0032	0.4697±0.0131	0.5032±0.0065	0.5747 ±0.0234	UWaveGestureLibraryZ	0.7324±0.0036	0.7591±0.002	0.7886±0.0013	0.8288 ±0.0021
Herring	0.6667±0.0239	0.7188±0.0271	0.6458±0.0239	0.724 ±0.009	Wafer	0.9903±0.0003	0.984±0.0069	0.9953±0.0004	0.9988 ±0.0005
HouseTwenty	0.9412±0.0	0.9496±0.0084	0.9356±0.0049	0.9776 ±0.0097	Wine	0.7901±0.0107	0.6049±0.0466	0.7593±0.0321	0.8148 ±0.0185
InlineSkate	0.363±0.0136	0.3182±0.0101	0.403±0.0211	0.4515 ±0.0132	WordSynonyms	0.5502±0.0081	0.4916±0.0113	0.6996±0.0063	0.7649 ±0.0027
InsectEPGRegularTrain	1.0 ±0.0	1.0 ±0.0	0.992±0.0	1.0 ±0.0	Worms	0.6537±0.027	0.7186±0.015	0.7662±0.013	0.7792 ±0.0026
InsectEPGSmallTrain	1.0 ±0.0	1.0 ±0.0	0.9665±0.0061	1.0 ±0.0	WormsTwoClass	0.8139±0.0198	0.8182±0.013	0.8225±0.027	0.8312 ±0.013
InsectWingbeatSound	0.519±0.0044	0.4791±0.0099	0.6222±0.0066	0.6246 ±0.0068	Yoga	0.815±0.0012	0.7472±0.0012	0.8308±0.0076	0.9087 ±0.0022
Blink	1.0 ±0.0	0.9963±0.0046	0.9896±0.0056	1.0 ±0.0	Handwriting	0.3392±0.01	0.4275±0.0107	0.3375±0.0129	0.482 ±0.0157
MotionSenseHAR	1.0 ±0.0	0.9962±0.0	0.9887±0.0	1.0 ±0.0	JapaneseVowels	0.9631±0.0056	0.9712±0.0016	0.9374±0.0165	0.9811 ±0.0054
SharePriceIncrease	0.6874±0.0	0.6746±0.0012	0.6891 ±0.0039	0.6874±0.0027	LSST	0.6054±0.0021	0.6718±0.0017	0.6944±0.0023	0.7109 ±0.0015
ArticularyWordRecognition	0.9933±0.0033	0.9933±0.0	0.9967 ±0.0	0.9933±0.0	Libras	0.8981±0.0085	0.8981±0.0116	0.937±0.0085	0.9388 ±0.0
BasicMotions	1.0 ±0.0	1.0 ±0.0	1.0 ±0.0	1.0 ±0.0	NATOPS	0.9074±0.0128	0.9333±0.0056	0.819±0.015	0.937 ±0.0116
CharacterTrajectories	0.9396±0.0008	0.9673±0.0021	0.9838±0.0029	0.9928 ±0.0004	PhonemeSpectra	0.2735±0.0078	0.2965±0.014	0.2415±0.0033	0.3421 ±0.0023
Cricket	1.0 ±0.0	0.9907±0.008	0.9861±0.0	1.0 ±0.0	RacketSports	0.9232±0.0038	0.9298±0.0076		

Table 8: The performance comparison between Mantis in the zero-shot feature extraction setting and when it is fully fine-tuned with or without an adapter, in average over UEA-27 datasets. In the second case, the best possible performance per dataset is taken.

dataset	RF	Full (Best Result)
ArticularyWordRecognition	0.9867 \pm 0.0076	0.9933 \pm 0.0
BasicMotions	0.9958 \pm 0.0102	1.0 \pm 0.0
CharacterTrajectories	0.9546 \pm 0.0165	0.9947 \pm 0.0004
Cricket	0.9884 \pm 0.0137	1.0 \pm 0.0
DuckDuckGeese	0.42 \pm 0.031	0.6 \pm 0.02
ERing	0.9549 \pm 0.0174	0.9926 \pm 0.0074
EigenWorms	0.7443 \pm 0.0172	0.8601 \pm 0.0192
Epilepsy	0.9915 \pm 0.0055	1.0 \pm 0.0
EthanolConcentration	0.2738 \pm 0.009	0.4208 \pm 0.0195
FaceDetection	0.5354 \pm 0.0119	0.6272 \pm 0.013
FingerMovements	0.5183 \pm 0.0354	0.6167 \pm 0.0058
HandMovementDirection	0.2635 \pm 0.0627	0.5135 \pm 0.027
Handwriting	0.2876 \pm 0.0569	0.5839 \pm 0.0283
Heartbeat	0.7626 \pm 0.0408	0.7951 \pm 0.0129
InsectWingbeatSubset	0.425 \pm 0.1992	0.591 \pm 0.005
JapaneseVowels	0.9216 \pm 0.0459	0.9811 \pm 0.0054
LSST	0.613 \pm 0.0084	0.7109 \pm 0.0015
Libras	0.8741 \pm 0.0297	0.9704 \pm 0.0032
MotorImagery	0.5483 \pm 0.0417	0.6 \pm 0.01
NATOPS	0.8648 \pm 0.0498	0.9611 \pm 0.0
PEMS-SF	0.9923 \pm 0.0119	0.9114 \pm 0.0067
PhonemeSpectra	0.2444 \pm 0.0322	0.3547 \pm 0.0047
RacketSports	0.8717 \pm 0.0569	0.9408 \pm 0.0
SelfRegulationSCP1	0.7793 \pm 0.0293	0.917 \pm 0.0052
SelfRegulationSCP2	0.4861 \pm 0.0331	0.5685 \pm 0.0251
SpokenArabicDigits	0.8872 \pm 0.0527	0.9933 \pm 0.0014
UWaveGestureLibrary	0.8432 \pm 0.0339	0.9438 \pm 0.0108